Islamic University of Gaza
Deanery of Graduate Studies
Faculty of Science
Physics Department

الجامعة الإسلامية - غزة
عمادة الدراسات العليا
كلية العلوم
قسم الفيزياء

Investigation of the Effect of Various Dyes on OLEDs Electroluminescence

BY

Hussam Sabri Musleh

Gaza

Palestine

Supervised By

Dr. Taher El-Agez

Assistant Prof. of Physics

"A Thesis Submitted in Partial Fulfillment of the Requirements for the Degree of Master of Science (M.Sc.) in Physics"

1430هـ - 2009 م

ABSTRACT

In this work, five sets of samples have been prepared and studied. Every sample represents an Organic Light Emitting Diode OLED. We used Poly(9-vinylcarbazole) (PVK) doped with different dyes (R6G, Alq_3, carbocyanine, oxadiazole and fluroscein) 2% concentration. The measurements include I-V characteristics and variation of relative light intensity with the driving voltage. The variation of relative light intensity with the current and the conduction mechanism have been studied.

The I-V characteristics are that of typical diode because the current increase exponentially with applied voltage. I-V characteristics and relative light intensity-voltage curves have approximately the same shape for the same sample. It is observed that, the lowest value of threshold voltage V_T was for (ITO/PVK R6G (blend)/Al) sample and the highest was for ITO/PVK 1,2,4 oxadiazole(blend)/Al) sample (see table(4.1)). In general, the values obtained for V_T are lower than those reported for conventional organic light emitting diode.

Electroluminescence-voltage characteristics curve reveals that the sample (ITO/PVK 1,2,4 oxadiazole(blend)/Al) is best sample exhibiting the maximum brightness which is achieved at an operating voltage of 10 V. By plotting the current-voltage curves in logarithmic scale, we ensured that the mechanism of conduction is ohmic at low voltage for all samples and at high voltage, space charge limiting conduction (SCLC) in most samples. Current-voltage in logarithmic scale curves demonstrate three regions for ITO/PVK R6G (blend)/Al, ITO/PVK carbocyanine(blend)/Al, ITO/PVK 1,2,4 oxadiazole(blend)/Al and four regions for ITO/PVK / Alq_3 /Al (double layer), ITO/PVK fluroscein (blend)/Al. The thicknesses of thin films were measured using homemade variable angle spectroscopic ellipsometer (VASE) .

We also deposited thin film of PVK (48 nm) on Si substrate, and another thin film (18 nm) of Alq_3 on Si substrate. We plot the variation of the refractive index of

a Alq_3 and PVK films with the variation of wavelength (visible spectrum). Finally, the experimental values of three Cauchy parameters (A, B, C) were calculated using a Matlab code.

الملخص العربي

لقد تم تحضير ودراسة فئات خمس العينات في هذا العمل. كل عينة تمثل ثنائي عضوي باعث للضوء OLED. حيث تم استخدام مادة عضوية تتمتع بالخواص الالكتروضوئية electroluminescence وهي PVK، التي طعمت بنسبة 2% بأصباغ dyes متنوعة مثل (Alq_3, R6G, fluroscein ,carbocyanine,1,2,4,oxadiazole)، وقد احتوت الدراسة علي دراسة علاقة كل من التيار كدالة في الجهد و كذلك علاقة شدة الإضاءة النسبية مع الجهد المطبق. وأيضا تم دراسة تغير الإضاءة النسبية مع تغير التيار والعلاقة بين اللوغاريتم الطبيعي للتيار مع اللوغاريتم الطبيعي للجهد.

وقد وجد أن جميع قياس توصيلية التيار المستمر I-V تعطي منحني الخواص للوصلة الثنائية. ولوحظ أن منحني I-V ومنحني (الجهد- الإضاءة النسبية) يأخذان نفس الشكل تقريبا للعينة الواحدة. وقد تم أيجاد قيمة جهد العتبة threshold voltage V_T لكل عينة. وكذلك لوحظ أن اقل جهد للعتبة كان في العينة (ITO/PVK R6G (blend)/Al) واكبر جهد للعتبة كان في العينة (ITO/PVK 1,2,4 oxadiazole(blend)/Al) (راجع جدول (4.1)) و هي قيم اقل من القيم التي تم الحصول عليها بنفس الطريقة ولقد وضحت العلاقة بين شدة الإضاءة النسبية والجهد أن العينة (ITO/PVK 1,2,4 oxadiazole(blend)/Al) أعطت أفضل إضاءة نسبية بالمقارنة مع غيرها من العينات حيث كان لها اعلي إضاءة نسبية عند 10V، وتم التأكد من أن التوصيل داخل جميع العينات عند الجهد المنخفض هو ohmic وعندما ترتفع قيمة الجهد المطبق علي العينة فان التوصيل يصبح لبعض العينات في بعض المراحل space charge limiting conduction ، وتم ذلك عن طريق رسم منحنيات التيار والجهد بالتدريج اللوغاريتمي الطبيعي current-voltage in logarithmic ولقد احتوت هذه المنحنيات للعينات S_1, S_3, S_4 ثلاثة مراحل (three region) أما في العينتين S_2, S_5 فقد احتوت علي 4 مراحل four (regions). كذلك تم قياس سمك بعض العينات باستخدام homemade variable angle spectroscopic ellipsometer (VASE).

وأخيرا تم تبخير غشاء رقيق من PVK فوق شريحة من السليكون Si وغشاء رقيق أخر من Alq_3 تم تبخير فوق شريحة أخري من السليكون Si و ذلك لدراسة تغير معامل الانكسار لنفس العينتين السابقتين مع الطول الموجي λ في المدي (400-650 nm) للضوء المرئي. ثم تم حساب القيم Cauchy parameters (A, B, C) باستخدام برنامج Matlab code (انظر جدول 4.3).

إهداء

إلى والديّ و والديّ

إلى زوجتي العزيزة و ابنتي "بلسم"

ACKNOWLEDGMENTS

All gratitude is due to God almighty who has ever guided and helped me to bring forth to light this thesis. I wish to express my deep gratitude and thanks to my supervisor Dr. Taher El-Agez, for suggesting the problems discussed in the thesis, for his continuous encouragement and invaluable help during my research. I am also grateful Dr. Ahmed Tayyan for his assistance in some discussion and helpful guidance throughout this work. I am also very grateful to my family for their encouragement.

CONTENTS

CONTENTS

CHAPTER ONE

Introduction

CHAPTER TWO

Organic Light Emitting Diodes (OLEDs)

CHAPTER THREE

Experimental Techniques

CHAPTER FOUR

Results and Discussion

LIST OF TABLES

LIST OF FIGURES

LIST OF SYMBOLES AND ABBREVIATIONS

Alq_3: 8-hydroxyquinoline aluminum.

Aqua Regia acid : (20% HCL, 5 % HNO_3).

CT: charge Transfer.

DIW: Deionized water.

$E(x)$: electrical field intensity.

E_i : quantized internal energy.

ETL: electron transport layer.

FPD: flat panel display.

HTL: hole transport layer.

HOMO: highest occupied molecular orbital.

h : Planck's constant.

k : Boltzman's constants.

N : charge density .

J : current density.

J_{dr} : drift current.

J_{df} : diffusion current.

ITO: indium tine oxide.

LUMO: lowest unoccupied molecular orbital.

OLED: organic light emitting diode.

PVK: Poly (9-Vinylcarbazole).

PPV: Poly(p-phenylene vinylene).

PFO: Polyfluorene.

RG6: Rhodamine 6G.

S: singlet state.

S: total electron spin angular momentum.

SCLC: Space Charge Limited Conduction.

T: triplet state.

TPD: (*N*,*N*_-diphenyl-*N*,*N*_-bis(3-methyl-phenyl)-(1,1_-biphenyl)- 4,4_-diamine).

THF: tetrahydrofloren.

ψ : the change in amplitude difference.

Δ : the change in phase difference.

e: electric charge.

μ : charge mobility.

D: diffusion constant.

ε : electrical permittivity.

r_s : Fresnel's reflection coefficient for S-component.

r_p : Fresnel's reflection coefficient for P-component.

Φ : work function.

χ^2 : the smaller difference between the calculated $(\psi_{calc}, \Delta_{calc})$ and the measured $(\psi_{\exp}, \Delta_{\exp})$.

V_T : threshold voltage.

LIST of APPENDIXES

Chapter One

Introduction

1.1 Introduction

The name of a polymer is usually derived from the name of a monomer by adding the prefix (poly). A polymer is a large molecule of many repeated units linked together to form a large chain. The first semi-synthetic polymer produced was Bakelite in 1909, and it followed by the first synthetic fiber, rayon, which was developed in 1911 [1,2,3]. The number of repeating units in the chain is called the degree of polymerization "n". The mass of a monomeric unit "M" multiplied by "n" gives the molecular mass of the polymer M_{pol} such that.

$$M_{pol} = n\,M \tag{1.1}$$

The degree of polymerization may vary through a wide range, from a few units to 100,000 units. Polymers with high degree of polymerization are called high polymers, but polymers which have low degree of polymerization are called oligomers [2]. If only one type of monomer is employed to form the polymer, the resulting molecule is called homopolymer. A Copolymer is obtained when two or more monomers are used to form a polymer [1,2].

1.2 Types of Polymer Molecular Structures

There are two main types of polymer molecular structures, homopolymers and copolymers.

1.2.1 Homopolymers

Homopolymers are polymers that consist of identical monomers. The molecular structure of homopolymers can be categorized into three main types: linear, branched, and Crosslinked (three dimensional) structure.

(a) Linear Polymer

Linear polymers are polymers with long chains, characterized by high degree of symmetry [3]. The main difference in linear polymer properties results from how the atoms and chains are linked together in space. Polymers that have one dimensional structure will have different properties than those that have two dimensional or three dimensional structure [1]. Denoting a monomeric residue by P, one would write the formula of linear polymer as shown in Figure (1.1).

Figure (1.1) Linear Polymers.

(b) Branched Polymer

A branched polymer is a long chain with side branches (side chains), the number and length of which may be very large [3]. This type is also known as a two dimensional polymers. A branched polymer is depicted in Figure(1.2) [2].

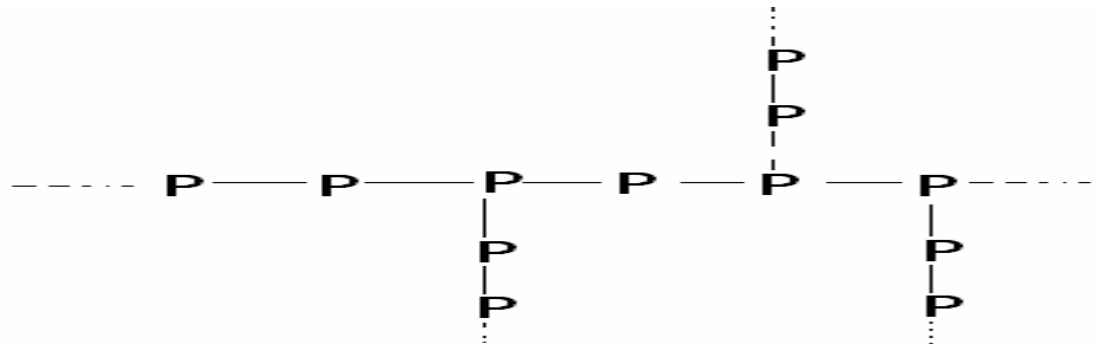

Figure (1.2) Branched polymer.

(c) Crosslinked Polymer

Crosslinked polymers consist of long chains connected up into a three dimensional network by chemical crosslink. Crystalline diamond and epoxy are good examples of three dimensional polymers. This structure offers low shear and good lubricating properties [1,4]. Figure(1.3). illustrates the structure of Crosslinked polymers.

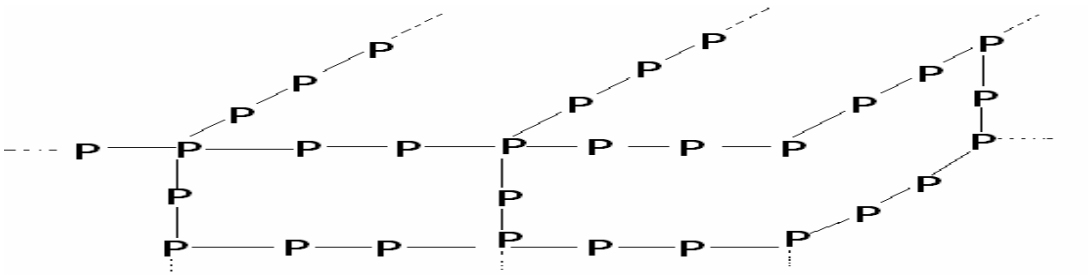

Figure (1.3) Crosslinked (three dimensional polymer).

1.2.2 Copolymers

Copolymers are polymers with at least two different types of monomers. Copolymers may be linear (random, alternating and block copolymer), branched or crosslinked molecule consisting of identical or different atoms. Linear copolymers in which the units of each form are fairly long with continuous sequences (blocks) are known as block copolymers as shown in Figure (1.4). A branched copolymers has a long chain of monomers of one kind in their main backbone and monomers of another type in their side branches. The structures of branched copolymers are shown in Figure (1.5) [1,2].

(a)

(b)

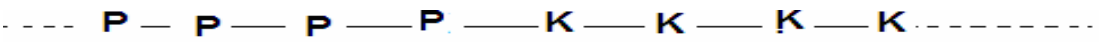

(c)

Figure (1.4) The three types of molecular structure (a) Linear random copolymer, (b) Linear alternating copolymer, and (c) Linear block copolymer.

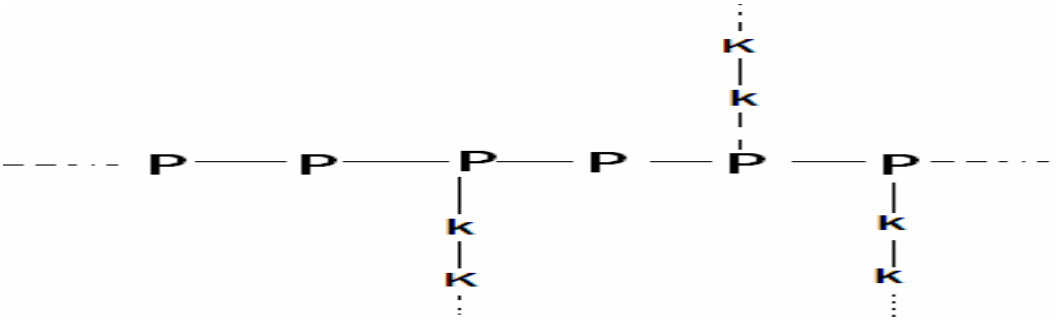

Figure (1.5) Branched copolymers

1.3 Conjugated Polymers

Conjugated polymers are polymeric compounds rich in electrons. The backbone of conjugated polymers consists of alternative double and single bonds at the same time. This alternativity plays an important role in the conductivity of the polymers [6]. The first and the simplest conjugated polymer is "polyacetylene" $(CH)_x$. Examples of conjugated polymers are polyacetylene, poly(p-phenylenevinylene), polyphenyl, polythienylenevinylene, polypyrrole, and polythienylenevinylene. The structures of these polymers are depicted in Figure (1.6).

Table (1.1) The HOMO/LUMO of some organic compounds used in OLEDs fabrication.

Compound	**Symbol chemical formula**	**HOMO (eV)**	**LUMO (eV)**
Poly (9-Vinylcarbazole)	PVK	5.8	2.3
8-hydroxyquinoline aluminum	Alq_3	5.8	3.1
(*N*,*N*_-diphenyl-*N*,*N*_-bis(3-methyl-phenyl)-(1,1_-biphenyl)- 4,4_-diamine)	TPD	5.4	2.4
Poly(p-phenylene vinylene)	PPV	5.2	2.7
Polyfluorene	PFO	5.8	2.9
1,2,4 Triazole	1,2,4 Triazole	4.7	1.7

The main characteristics in conjugated polymers are their low bandgap between highest occupied molecular orbital (HOMO) and lowest unoccupied molecular orbital (LUMO). When a molecule absorbs light of suitable wavelength, an electron is excited from its HOMO to the LUMO. Bandgaps in materials can be expressed by the energy difference between HOMO and LUMO levels. The HOMO and LUMO of some organic compounds used in OLEDs fabrication are listed in Table (1.1) [6, 7].

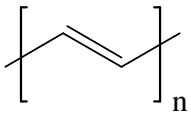

(a)

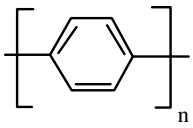

(b)

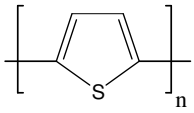

(c)

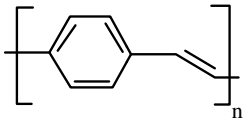

(d)

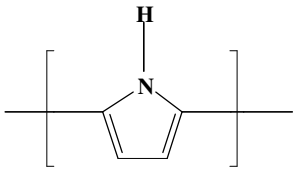

(e)

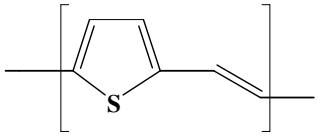

(f)

Figure (1.6) Representative $\pi-$ conjugated polymers in their pristine form (a) Polyacetylene, (b) Polyphenyl, (c) Polythiophene (d) Polyphenylenevinyle, (e) Polypyrrole, and (f) Polythienylenevinylene.

1.4 Molecular Orbitals

Molecular orbitals are formed by overlap of atomic orbitals. Every electron in a molecular orbital has a particular energy state. For example, in hydrogen molecule H_2, the energy of electron in bonded molecular orbital (BMO) is less than its energy in atomic orbital Ψ_{1s}. In contrast, the energy of an electron in antibonding molecular orbital is greater than its energy in atomic orbital. Figure (1.7). illustrates the energy diagram for molecular and atomic orbitals for hydrogen molecule H_2. There are two electrons with opposite spins placed in the bonding molecular orbital. Also, in the atomic orbitals one electron has spin up and the other has spin down. However the total energy of the two electrons together in (BMO) is less than that in atomic orbitals [8]. The energy of $\Psi_{molecular}$ orbital which has two electrons is lower than energy of $\Psi^*_{moleculer}$ orbital which has no electrons. For example, when the hydrogen molecule absorbs enough energy of a photon in high energy (ultraviolet), then the molecule is excited and the electron occupies the antibonding orbital. This case is called the excited state of the hydrogen molecule [8,9].

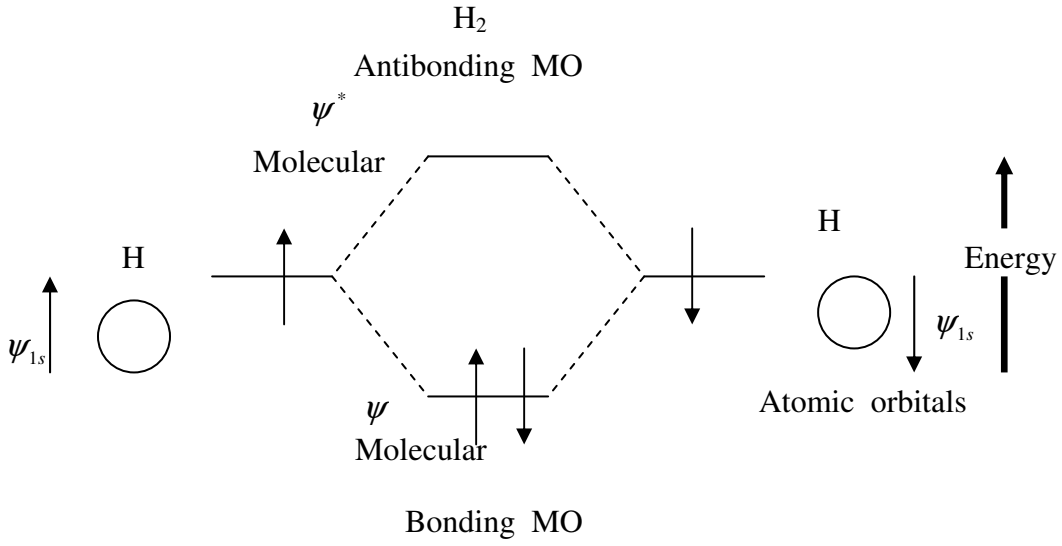

Figure (1.7) Energy diagram for the hydrogen molecule.

1.4.1 Singlet State

In this case there are one pair of electrons in the molecular orbital, one is spin up (+1/2) and the other is spin down (–1/2), this means that the total electron spin angular momentum **S**= $s_1 + s_2 = -1/2 + 1/2 = 0$. In general the multiplicity = (2x **S**) +1= 1 "singlet".

1.4.2 Doublet State

When the electron in molecular orbitals is not paired (one electron) this means that the total spin **S**= $s_1 = 1/2$ and the multiplicity = (2 x1/2) + 1 = 2 "doublet". The hydrogen atom is a good example for doublet state.

1.4.3 Triplet State

In triplet state there are two "spin-up" electrons. i.e. two electrons of the same spin, +1/2 and +1/2. Total electron spin angular momentum, **S**=1and the multiplicity = (2 x1) +1=3 "triplet".

1.5 The Internal Energy of Molecules

The molecular internal energy of a molecule in the electronic state is the sum of the rotational, vibrational and electronic energy transitions. The internal energy E_{int} of a molecule in its electronic ground or excited state can be expressed by the following equation:

$$E_{\text{int}} = E_{el} + E_{vib} + E_{rot} \tag{1.2}$$

where E_{el} is the electronic energy, E_{vib} is the vibrational energy and E_{rot} is the rotational energy [10].

1.6 Absorption Processes

When the molecule absorbs external energy of a photon ($E = hc/\lambda$) of

suitable λ . where h is Planck's constant, c is the speed of light and λ is the wavelength, the molecule becomes excited. Each one of the electronic states (ground or excited) has a number of vibrational and rotational levels. This energy approximately equals the energy difference between the ground state and the excited state equivalent to energy difference between HOMO and LUMO molecular states. In general, molecules absorb wide range of wavelengths, a broad band rather than one single wavelength. In the absorption process the transitions from ground state S_0 to the first and second excited singlet state S_1, S_2 are allowed, but the direct transition from the ground state S_0 to the triplet state T_1 is forbidden [10,11].

1.7 Fluorescence and Phosphorescence

Luminescence is the emission of light. It is emitted after the electrons return from the first excited singlet state S_1, and the first excited triplet state T_1 to the ground state S_0 and loses its excited energy as fluorescence and phosphorescence, respectively.

1.7.1 Fluorescence

Absorption of UV or visible radiation of suitable λ by a molecule leads to excitation. The electrons jump to the different vibrational states in S_1. The electrons in S_1 can then undergo vibrational relexations and return to the main excited electronic levels then return to S_0 giving luminescence known as fluorescence. The life time of electrons in S_1 between 10^{-9} to 10^{-7} second, which is a very short time. But, when the molecule absorbs energy less than the difference energy between the ground state and the first excited state, the energy is used in making vibrations and rotations of the molecule in the ground state with radiationless process. The quantum yield (for fluorescence) depends on the ratio of the number of emitted photons and the number of absorbed photons. Let A^* be the excited state of the molecule, the following equation represents the fluorescence emitted from the excited molecule.

$$A^* \quad \rightarrow \quad A + h\nu \tag{1.3}$$

where A represents the molecule after losing the energy and ν is the frequency of the emitted radiation. The amount of radiation emitted as fluorescence is lower than the average amount absorbed by a molecule, because part of the energy was used in making vibrations and relaxations of electrons to main electronic level [12,13].

1.7.2 Phosphorescence

When the electrons are in the excited state S_1, they may be transferred by intersystem crossing ISC to reach one of vibrational levels of the first excited triplet state T_1. Some vibrational relaxations occur, then the electron undergoes a second flip in spin and returns to the ground state S_0 with luminescence emission. This phenomena is known as phosphorescence. The life time of triplet state is nearly equal 10^{-4} s to several seconds. The transition between triplet state and the ground state is called Singlet-Triplet transition which is less probable than Singlet-Singlet transition. Various radiation and radiationless transitions which occur in molecules are shown in Perrin-Jablonski diagram in the Figure (1.8) [12]. State S_0 is the ground state, S_1 is the first excited singlet state, S_2 is the second excited singlet state. IC is the internal conversion, which is transitions between states with the same spin. For example the transition between S_2 to any vibrational level in S_1. ($S_2 \rightarrow S_1$, $S_1 \rightarrow S_0$). ISC is the intersystem crossing, where the transition between the states with different spins occurs. Phosphorescence dyes possess strong intersystem crossing (ISC) from the excited singlet state to the triplet state ($S_1 \rightarrow T_1$). Little or no fluorescence is observed in these materials.

Singlet–singlet absorption results in the transition from the singlet ground state of the molecule into the singlet excited state ($S_0 \rightarrow S_n$) and leads to the UV/VIS absorption spectrum. The analogous triplet absorption takes place in the transition from the lowest triplet state of the molecule to a higher state ($T_0 \rightarrow T_n$), thus leading to the triplet-triplet absorption spectrum. In general the transition between energy states with the same multiplicity is allowed and exhibits radiation, but the transition is not allowed when the transition between energy states has different multiplicity, this is called the spin conservation rule[10]. In general phosphorescence is distinguished from fluorescence by the speed of electronic transition that generates luminescence. Both processes require the relaxation of an excited state to the ground state. Fluorescence and Phosphorescence materials are very important to improve the efficiency of OLEDs luminescence, because the main characteristics of OLEDs luminescence depend on these materials [13].

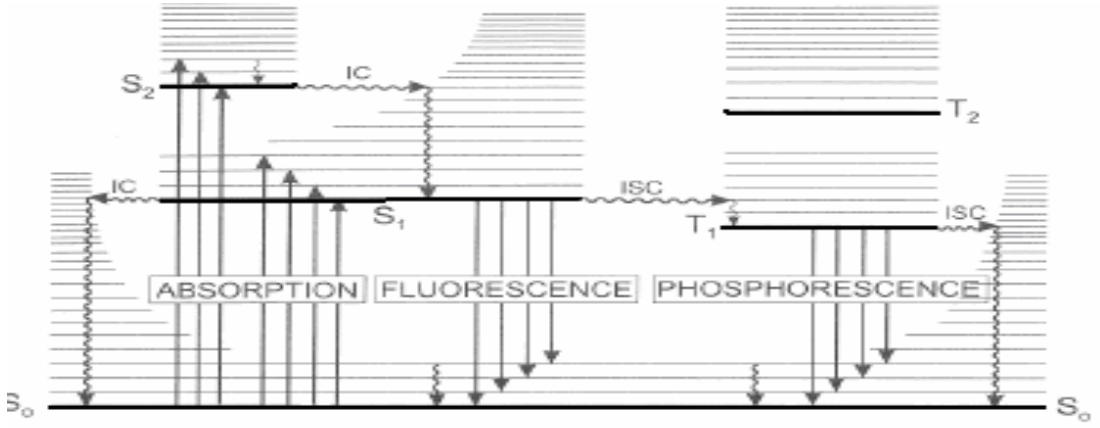

Figure (1.8) Perrin-Jablonski diagram and illustration of the relative positions of absorption, fluorescence and phosphorescence spectra.

1.8 Exciton

The exciton is defined as a combination of an electron and a hole. The exciton is treated in calculations as a chargless moving particle which is able to diffuse and carry excitation energy. It behaves like a neutral particle moving through media. An exciton may decay and emit luminescence with radiative decay, or decay without luminescence [14,15,16].

1.8.1 Classification of Excitons

There are two main types of excitons, Wannier excitons and Frenkel excitons [14]. Each type has specific characteristics, e.g. localization, binding energy and radius of exciton (distance between hole and electron).

Wannier excitons has a radius much larger than the lattice spacing (constant distance between unit cells in crystal lattice). It is found in dense media like crystals and inorganic semiconductors. The binding energy (between hole and electron) of Wannier exciton on the order 0.1 eV. The size of exciton in this case is larger than other exciton such as Frenkel exciton.

Frenkel exciton is found in the materials which have very small dielectric constant ε such that in organic semiconductors. It is a highly localized exciton and the coulomb's interaction force between hole and electron is very strong, so the exciton tends to be

much smaller. The binding energy of Wannier exciton about 1.0 eV. Figure (1.9). illustrates a Wannier exciton and a Frenkel exciton [14,16].

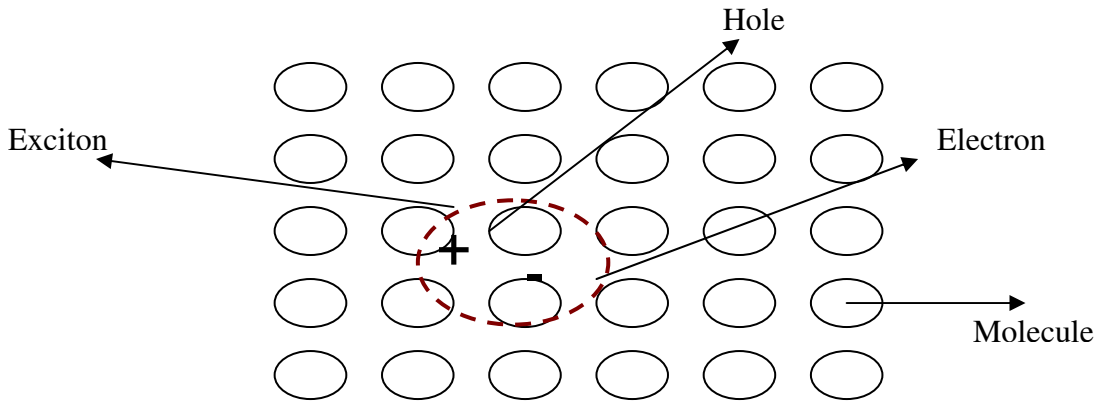

(a)

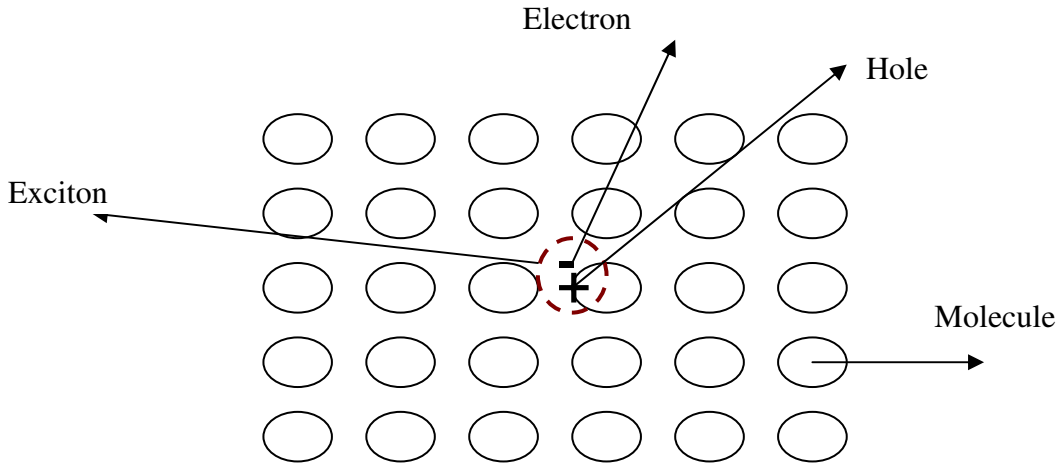

(b)

Figure (1.9) The spatial discrimination of excitons (a) Wannier exciton, (b) Frenkel exciton.

1.9 Energy Transfer

There are two main forms of energy transfer mechanisms, Fŏrster and Dexter mechanisms, both of them are non radiative energy transfer**.** The basic mechanism of Fŏrster and Dexter transfer in light emitting diode (OLED) can be illustrated with two organic materials, one a net electron donor (D) and the other an acceptor (A).

1.9.1 Fŏrster (Singlet- Singlet) Transfer

Fŏrster transfer is (singlet-singlet) radiationless transfer process, which, therefore, does not involve emission of the light from the donor molecule at any stage. Fŏrster transfer occurs in very short time less than 10^{-9} second. There is a Columbic interaction of the dipoles of two molecules, excited doner molecule D* and the acceptor of the excited molecules A. The movement of the excited electron on the donor molecule creates an oscillating dipole. Figure (1.10). shows the Fŏrster transfer [16,17].

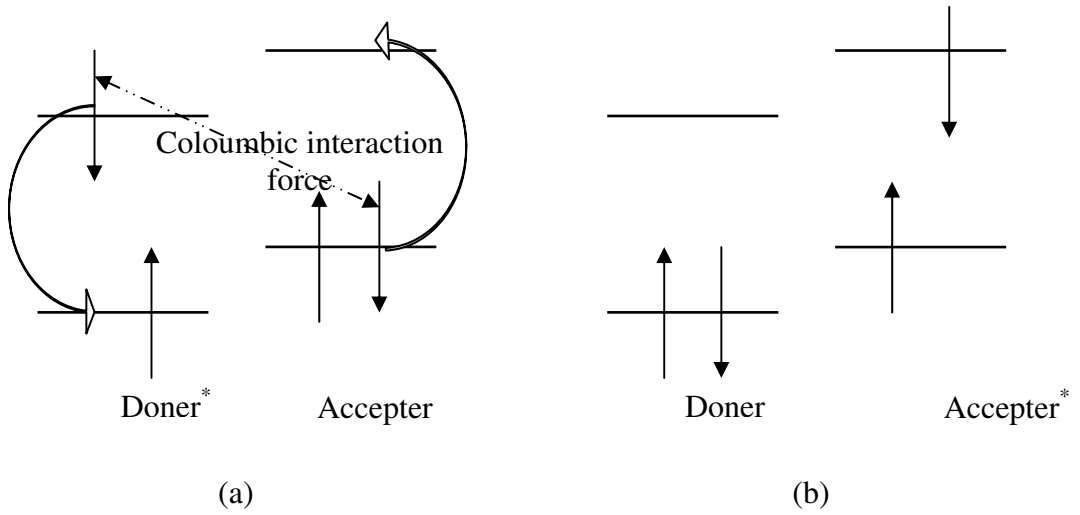

Figure (1.10) Fŏrster (singlet) transfer, (a) The initial state, (b) The final state.

1.9.2 Dexter (singlet- singlet or triplet-triplet) Transfer

The most common exciton is the so called Dexter exciton which is a strongly bound, electron-hole pair usually localized on a single molecule. The mechanism of the Dexter transfer is an electron exchange (tunneling) process. Where the donor excited electron in the excited state (jump) to the excited state of the acceptor A and

one of the electron in the ground state of the acceptor A jumps to the ground state of the donor molecule D as shown in Figure(1.11). The two exchanges may occur either simultaneously, or one after the other. The rate of Dexter mechanism transfer is also exponentially dependent on the distance between the donor and the acceptor. In Dexter transfer singlet- singlet or triplet-triplet transitions are allowed, 25% of the formed excitons will be singlets and 75% will be triplets. This is because the triplet state has three spin projections (Ms = 0, ±1) and the singlet has only one (Ms = 0) [16,17].

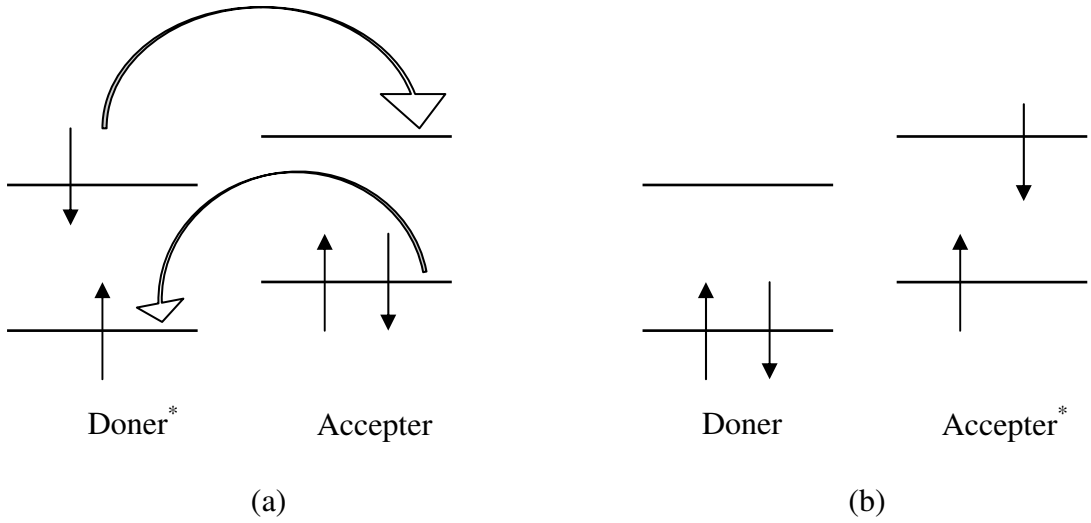

Figure (1.11) Diagrammatic representation of Dexter energy transfer, (a) The initial state, (b) The final state.

1.10 Poly N-Vinylcarbazole (PVK)

1.10.1 Carbazole

Carbazole is an aromatic tricyclic compound which was discovered in 1872 by Graebe and Glaser from the coal tar [19]. A high number of carbazole monomers linked together will form poly(vinylcarbazole) compound. The chemical structure of carbazole is illustrated in Figure 1.12(a). Pure carbazole is a white crystalline organic material which has melting point of 246 ^{0}C, and 167.2 g/mole molecular weight. Carbazole has high boiling point compared with many of organic materials [14]. It is an electroluminescent material. Carbazole emits strong fluorescence and long phosphorescence by exciting with enough energy (ultraviolet) [19,20].

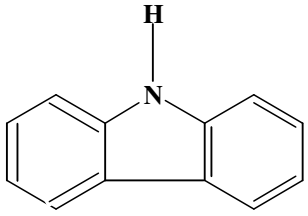

(a)

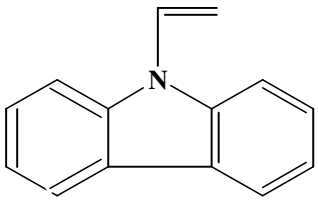

(b)

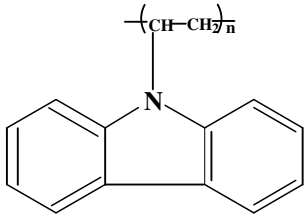

(c)

Figure (1.12) The structure of, (a) Carbazole,(b) N-vinylcarbazole, (c) and Poly(N-vinylcarbazole).

1.10.2 Poly (9-Vinylcarbazole)

Poly(9-vinylcarbazole) (PVK) is tricyclic organic polymeric material which is transparent plastic material. The softening point of PVK is nearly a 175 ^{0}C and glass transition temperature (Tg) is at 211^{0}C. The chemical structure of PVK is illustrated in Figure 1.12(c). the solubility of PVK is very strong in alcohol, ether and THF. Usually PVK films are deposited by spin coating. It has good optical properties, PVK has a strong photoconductive and electroluminescence properties. It has a high refractive index ~1.69 in the visible region. Electrically, PVK is an insulator in dark but under the ultraviolet radiation, it exhibits electro-conductivity. Commercially PVK is used as a paper capacitor, in OLEDs, data storage, sensors and transistors. In OLEDs, PVK is used as a hole transport material[20].

1.11 Indium Tin Oxide (ITO)

Indium tin oxide (ITO, or tin-doped indium oxide) is a mixture of indium oxide (In_2O_3) and tin oxide, typically 90% In_2O_3, 10% SnO_2 by weight. Most of ITO coated glass is available in surface resistivities from 5Ω/□ to 1000Ω/□. ITO is used widely for optoelectronic devices because it exhibits a good electrical conductivity with high transparency in the visible range. ITO electrodes are used in interesting applications such as heat reflecting mirrors, high temperature gas sensors, thin film solar cells and OLEDs. In addition it can be used as a positive electrode in flat panel displays. The deposition of ITO on a flat glass substrate is achieved by using sputtering or spray techniques. Sputtering involves knocking an atom or a molecule out of the target material by accelerated ions from an excited plasma, then depositing ITO thin film onto high quality glass substrates [21].

Chapter Two

Organic Light Emitting Diodes (OLEDs)

2.1 Introduction

In this chapter we present an introduction to OLEDs and an overview of emission mechanism of light from an OLED . Then, we shall discuss and derive ohmic and Space Charge Limiting (SCLC) conduction models which may take place during operation.

An OLED consists of thin films of electroluminescent organic layers (single or multiple layers) sandwiched between two electrodes. By applying a suitable voltage, electroluminescence is emitted through the transparent electrode. The first OLED was prepared in 1987 by C.W Tang and Van Slyke [22]. This device consists of two layers, the first layer was an aromatic diamine which acts as a hole transport layer (HTL). The second layer was an emissive layer 8-hydroxyquinoline aluminum (Alq_3). The chemical structure of diamine and (Alq_3) are illustrated in Figure (2.1). The structure of the first OLED is depicted in Figure (2.2) where the anode is an Indium-Tin-Oxide (ITO) film deposited onto glass substrate. The ITO electrode is a transparent electrode that transmits light emitted from the device. The other electrode is usually an aluminum layer which acts as the cathode of the device. Other materials such as Ag, Mg and Ag/Mg(alloy) may be used as a cathode [22,23].

Many conjugated polymers are used in OLEDs fabrication to exhibit electroluminescence with different colors [23].

2.2 Mechanism of Light Emission From an OLED

An OLED is a device which consists of one or more organic thin films sandwiched between two electrodes. The transparent electrode is an ITO anode with a work function that is higher than that of the cathode. The work function of ITO is equal to 4.7eV while the work function of Al is equal to 4.3 eV. This difference in work functions creates potential and energy difference between the two electrodes. The work function of some materials used in OLEDs fabrication is tabulated in Table (2.1) [24,25]. When a suitable bias is applied between the two electrodes of the OLED, holes are ejected from the anode (source of holes) into the highest occupied molecular orbital (HOMO) of the hole transport layer (HTL). In the opposite electrode, electrons are ejected from the cathode into the lowest unoccupied molecular orbital (LUMO) of the electron transport layer (ETL).

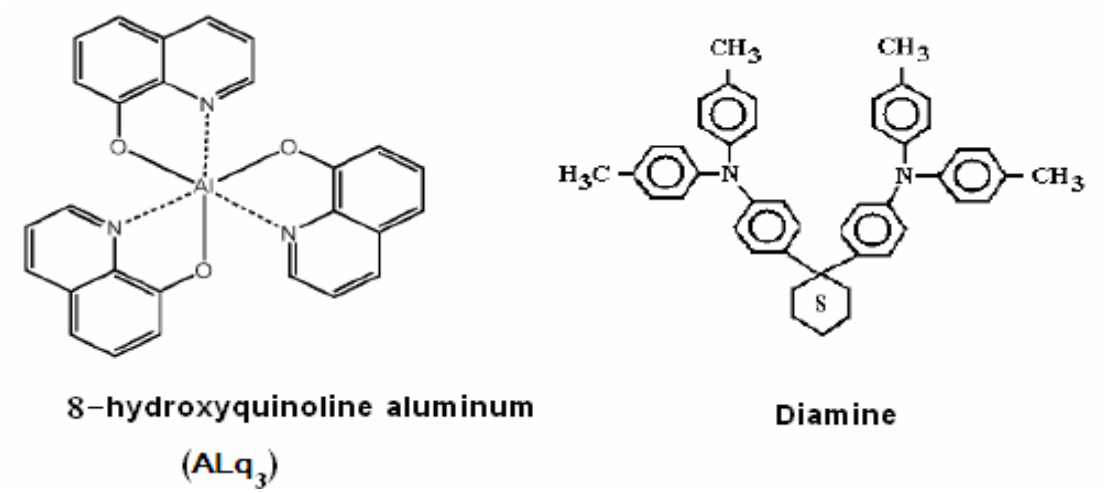

Figure (2.1) Alq_3 and diamine molecular structures.

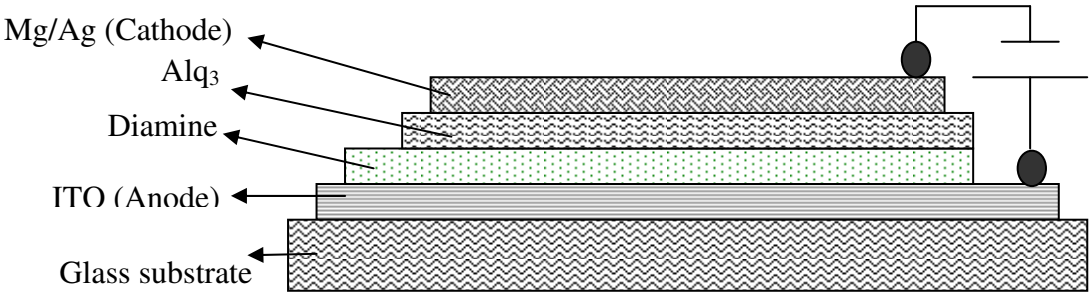

Figure (2.2) The first OLED which was fabricated by C.W Tang and VanSlyke.

The electrons and holes transport in the organic material and recombine to create a lot of excitons. Some of the excitons decay radiatively to give electroluminescence and others decay with radiationless process. The recombination of holes and electrons is responsible for the OLED light output in the ETL near the ETL/HTL interface. Figure (2.3) presents the mechanism of electroluminescence emitted from an OLED.

A lot of enhancements can be done to increase the internal quantum efficiency of OLED performance. The internal quantum efficiency is defined as the ratio of the

number of photons produced within the device to the number of electrons flowing from the external voltage. To achieve an efficient luminescence, it is necessary to have a good balance of electrons and holes within the emissive layer. A hole blocking thin film is deposited under the electron injection layer to increase the population of holes in the emissive layer. Dopping of the emitter layer with an organic dye molecules allows energy to transfer from the emitter molecule (host) to the dye molecule (guest) in order to increase the luminance efficiency or to tune the wavelength λ of the emitted electroluminescence [22]. The efficiency of the device not only depends on the electrical and optical properties of materials but also depends on the device structure single or multi layers. The performance of double layer OLED is better than that of single layer. This behavior is attributed to the long time spent by the charge carriers (electrons and holes) in the polymeric layers which increases the creation the excitons inside polymeric layers. In the single layer, most of holes and electrons have less chance to stay inside the polymeric layers. This facilitates the motion of holes to cathode and the motion of the electrons to anode [24].

Table (2.1) The work function Φ of some materials.

Material	**Work Function Φ (eV)**
ITO	4.70
Al	4.30
LiF	4.29
Ca	2.87
C	5.00
Au	5.10
Mg	3.66
Ag	4.26

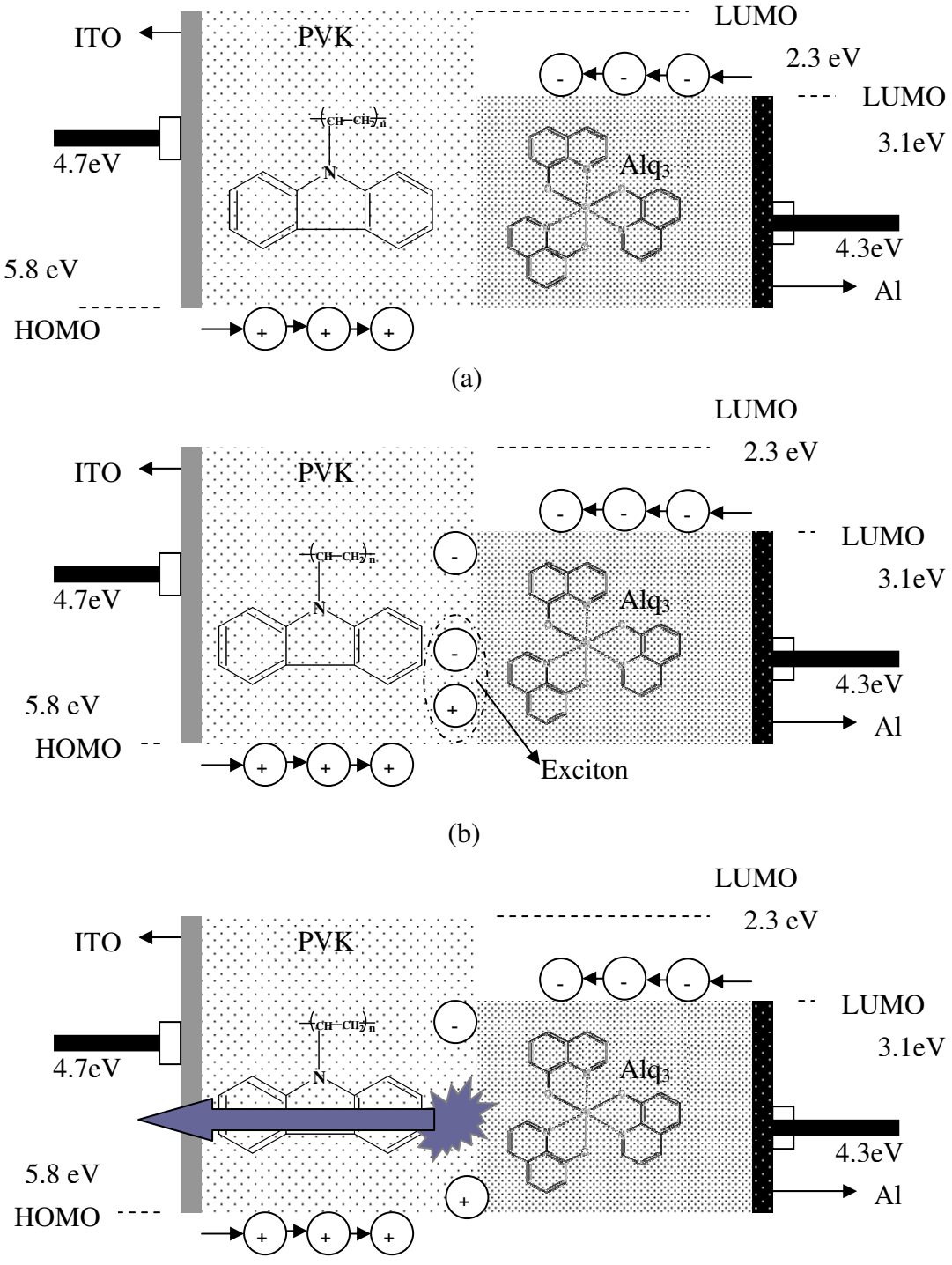

Figure (2.3) Mechanism of electroluminescence of a PVK / Alq_3 OLED (a) Injection and transporting of electrons and holes from cathode and anode respectively (b) Formation of exciton (c) Exciton decay radiatively to produce electroluminescence.

2.3 Conduction

2.3.1 Space Charge Limited Current (SCLC)

Space Charge Limited Current (SCLC) occurs when the current is limited by the space charges. The occurrence of space charge limited current requires that at least one contact has good injecting properties to provide an inexhaustible carrier reservoir. SCLC in a device can occur if at least one contact is able to inject more carriers than the metal has in thermal equilibrium without carriers injection. When the equilibrium charge concentration (before charge injection) is negligible compared to the injected charges concentration this will form a space charge cloud near the injection electrode. In general, the DC current of device can be divided into two main regimes, ohmic regime and space charge regime. In the ohmic regime, the current is linearly proportional to the electric field [26,27] as shown in equation (2.1).

$$J \propto E \qquad (2.1)$$

In the second regime (SCLC), the current is proportional to the square of the electric field

$$J \propto E^2 \qquad (2.2)$$

2.3.2 MOTT- Gurney Steady-State Space- Charge-Limited Conduction Model

The Mott-Gurney expression for (SCLC) was developed for a constant mobility. Verifying the SCLC region is an essential part of our experimental methodology fragment [27,28]. The space charge limited conduction current density J in a dielectric sample is proportional to the a square of the applied voltage V. A special case arises when the current is limited by the space charges. This means that the density of free carriers injected into the active region is larger than the number of acceptor levels. The entire current only comes from the diffusion of carriers. In other words, the current is caused by the large gradient of density of free carriers.

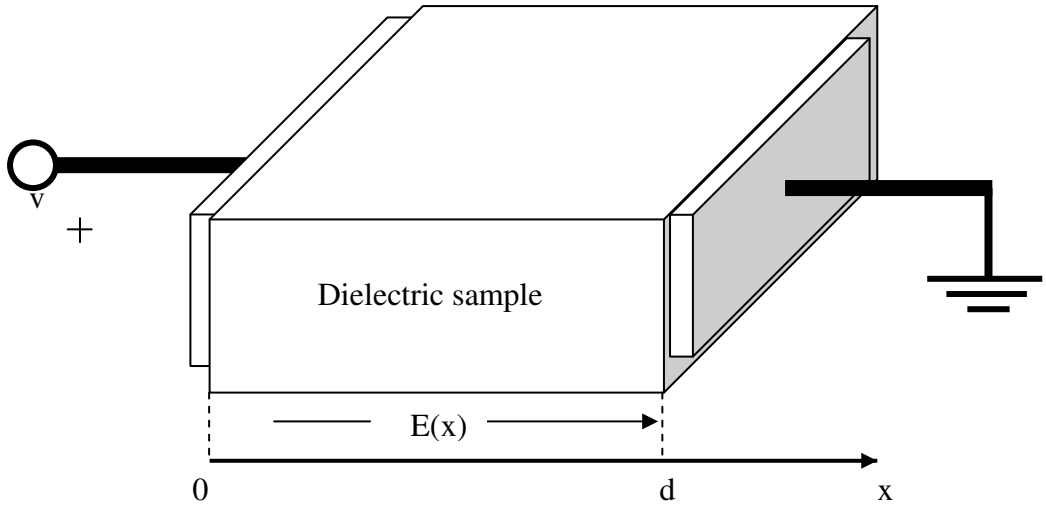

Figure (2.4) Current density J of dielectric sample with permittivity ε and thickness d in the x-direction.

The drift current (J_{dr}) is related to the electric field (in x-direction) by

$$J_{dr} = Ne\mathrm{v} \tag{2.3}$$

where

$$\mathrm{v} = \mu E(x) \tag{2.4}$$

substituting from equation(2.4) into equation(2.3), J_{df} becomes

$$J_{dr} = Ne\mu\ E(x) \tag{2.5}$$

and the diffusion current (J_{df}) is given by [29,30]

$$J_{df} = De\frac{d}{dx}N \tag{2.6}$$

where J is the current per unit cross-sectional area, N is charge density, e is the electronic charge, v is the drift velocity, E(x) is the electrical field in the x-direction, μ is the charge mobility, and D is the diffusion constant of electrons in m^2/sec.

The total current density J is given by

$$J = Ne\mu_P E(x) + De\frac{d}{dx}N \tag{2.7}$$

The exact theory of SCLC is rather complicated. The simplified theory neglects the diffusion current. So, the current density is given by equation (2.5) and the Poisson equation (in x- direction) can be expressed as

$$\frac{d}{dx}E(x) = \frac{e}{\varepsilon}N \tag{2.8}$$

where ε is electrical permittivity of the media.

substituting equation (2.8) into equation (2.5) we get

$$J = \varepsilon\mu_P E(x)\frac{d}{dx}E(x) \tag{2.9}$$

After some manipulation (see appendix A)

$$V = \int_0^d E(x)\ \ dx = \sqrt{\frac{8J}{9\varepsilon\mu}}\{(d+\kappa)^{\frac{3}{2}} - \kappa^{\frac{3}{2}}\} \tag{2.10}$$

we may have two cases

- Case one, for $\kappa << d$ equation (2.10) becomes

$$V = \sqrt{\frac{8J}{9\varepsilon\mu}}\ d^{\frac{3}{2}} \tag{2.11}$$

squaring both sides

$$J_{SCL} = \frac{9}{8}\mu\varepsilon\frac{V^2}{d^3} \tag{2.12}$$

Equation (2.12) shows Space Charge Limited regime.

where, V is the applied voltage, and d is the thickness of the layer.

- Case two, for $\kappa >> d$ equation (2.10) becomes

$$J_{ohm} = Ne\mu\frac{V}{d} \tag{2.13}$$

Equation (2.12) show that, in space charge limiting conduction there is a limit to the maximum amount of positive or negative charge that can be injected to the device. But in ohmic conduction, there is no barrier to the injection of charge into organic film as described in equation (2.13) [29,30,31].

Chapter Three

Experimental Techniques

3.1 Introduction

This chapter explains the different experimental techniques involved in the fabrication of OLEDs which are studied in this work. It includes description of etching ITO substrates followed by spin coating. A cathode is then deposited by thermal vacuum evaporation using shadow mask as shown in Figure (3.3). A homemade variable angle spectroscopic ellipsometer (VASE) was used to determine the thickness and the refractive index (n) of the organic thin films.

3.2 Sample preparation

3.2.1 Etching of ITO Substrates

The starting substrates consist of ITO coated glass sheets (7.5cm x 2.5cm) were purchased from delta technologies, USA. A digital multimeter (Fluke77) was used to determine the conductive surface of ITO substrate. Each sheet was cut into small pieces with dimensions 2.5 cm x 2.5 cm by using diamond scribe. Every sample was arranged in an 4 x 4 array of devices. The ITO substrates (electrodes) were cleaned thoroughly by wiping each electrode surface by a cotton pad wetted with acetone. Then, an electric tape is stuck at the conductive side of the ITO coated glass substrate. ITO electrodes were then etched to form the desired pattern by immersing them in a Aqua-Regia acid (solution of 20% HCl and 5% HNO_3) for 15 minutes at 60 °C. A digital multimeter (Fluke77) was used to measure the resistance of the etched regions of the ITO substrates. Very high resistance must be recorded if the etching procedure is successful in removing all the ITO onto etched regions of the glass substrates. After etching, the tape was removed and the patterned samples were rinsed in DI water to remove away the leftover acids. The etched ITO plates were then rubbed with a lens paper to remove tape residue. Upon completing the etching process, the substrate must be cleaned using DC arc plasma for 8 minutes [23].

3.2.2 Spin Coating

Spin coating is a technique widely used to deposit thin films of organic materials on top of flat substrate using a spin coater. In general, a spin coater consists of a table, which has very smooth surface, mounted on very fast motor with multi-angular speed. The thickness of the film depends on the rotational speed, viscosity, surface tension, drying rate, percent of the solids, and spin time. In spin coating technique, the solution must be homogenous, have no solid species, and the substrate must be clean.

There are three steps to do spin coating. The first step is fixing a clean substrate horizontally on to the center of the bench of spin coater clip and an amount of a polymer solution is placed on the substrate to be coated. In the second step, the substrate is rotated at a constant rate to achieve the final speed in order to spread the fluid by centrifugal force. Rotation is continued for known time and the fluid being spun off the edges of the substrate, until the desired film thickness is achieved. In the third step, the solvent usually volatiles and the solution condenses in a form of thin film on the substrate surface. The main three steps of spin coating process are depicted in Figure (3.1). During the spinning process, care must be taken to obtain a dust free film. The film thickness is controlled using different speeds. Thin films require high spin speed and long spin time but thicker films require short spin time and low spin speed [32].

3.2.3 Thermal Vacuum Evaporation of Organic and Cathode Layers

The deposition of the organic layers and the cathode of each samples are performed in a vacuum chamber by heating the materials electrically in vacuum until evaporation. A schematic setup of the thermal evaporator is depicted in Figure (3.2). The glass substrate is mounted to a holder with ITO substrate facing a basket in which the organic material is placed for thermal evaporation. The ITO substrate must be mounted as quickly as possible after the cleaning and etching procedures to avoid contamination with dust particles. Edwards Diffstak 100 water-cooled diffusion pump was used to pump down the chamber to a low pressure of about 10^{-5} torr range.

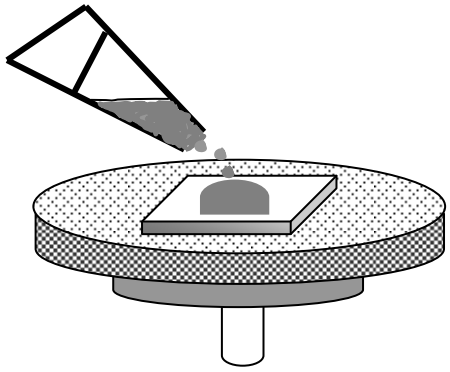

(a)

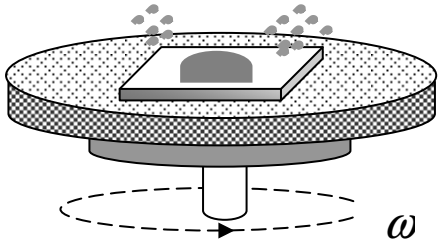

(b)

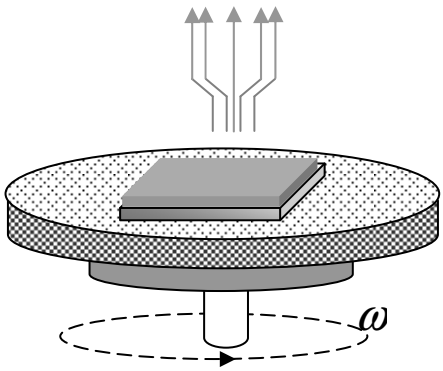

(c)

Figure (3.1) Spin coating steps (a) Dispensing, (b) Spreading, and (c) Drying.

After reaching a suitable pressure, indicated by the monitor, the hot resistance could be switched on for a suitable time to evaporate the material inside the boat. The shadow mask, which has 5 fingers as shown in Figure (3.3), is used in order to define four separate cathode contact to the OLED. Aluminum is used to make the electrodes in our samples. It is deposited by thermal evaporation deposition technique. After the chamber reaches vacuum pressure about 10^{-5} torr. The aluminum is heated until fusion, using electrical current passing through tungsten coil for one minute. When the evaporation is completed, the diffusion pump is closed and the sample is removed outside the bell jar. We used aluminum as the cathode of OLED samples due to its stability compared with calcium or magnesium [33,34].

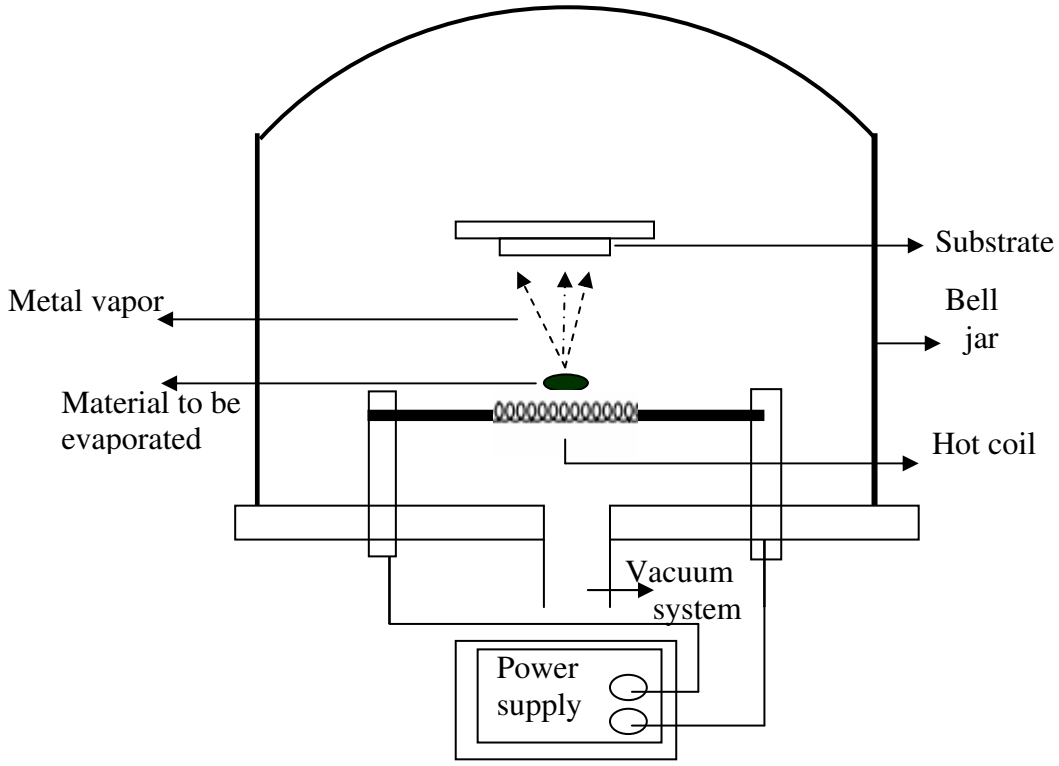

Figure (3.2) A schematic setup of thermal evaporator

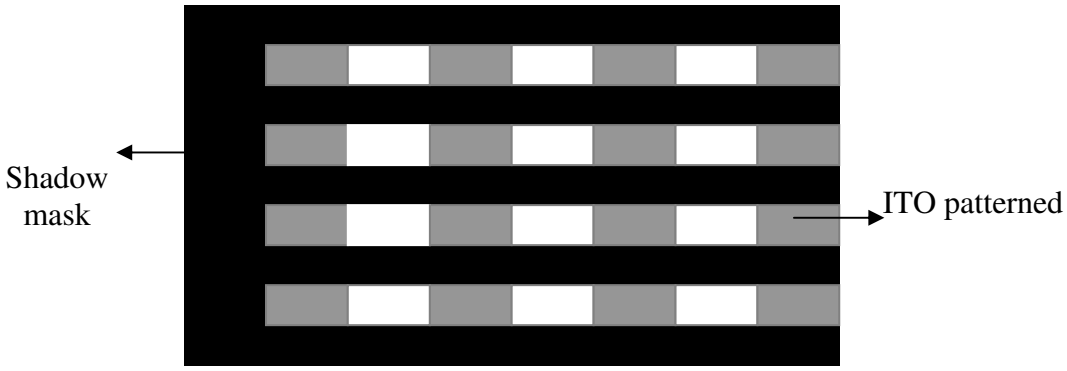

Figure (3.3) Shadow mask is placed on top of ITO substrate

3.3 Experimental Setup

3.3.1 Samples

Five OLED samples were prepared in this work. One of these samples consists
of a double layer ITO/PVK/ Alq_3 /Al. The other OLEDs are single layer type doped with various dyes. These samples are listed in table (3.1).

Table (3.1) The name and the structure of all samples.

Sample name	Structure of the sample
S_1	ITO/PVK R6G (blend)/Al
S_2	ITO/PVK / Alq_3 /Al (double layer)
S_3	ITO/PVK carbocyanine(blend)/Al
S_4	ITO/PVK 1,2,4 oxadiazole(blend)/Al
S_5	ITO/PVK fluroscein (blend)/Al

3.3.2 Experimental Procedure

The general structure of the single layer samples is (ITO/doped polymer film/Al). An amount of 300 mg of Poly(9-vinylcarbazole) with an average molecular weight of $11x10^5$ (purchased from Sigma-Aldrich, USA) was dissolved in 150 CC THF. A 2% by weight of the dye was added to the solution. PVK and the dopants were weighted by using a sensitive electrical balance (sartorious AG Goettingen model BA1105) with a resolution of 10^{-4} gm. Poly(9-vinylcarbazole) was dissolved in a proper amount of organic solvent such as THF. The desired weight concentration of the dopants were then added to the solution. The solution was then stirred thoroughly and filtered. For the single layer samples, few drops of the blend solution were spun at 1750 rpm for one minute to form thin film on the etched ITO.

For the double layer sample, the Alq_3 layer was deposited on the PVK film using thermal vacuum evaporation at $1.7x10^{-5}$ torr in low rate deposition condition for one minute. The samples were then stored in an oven at 80^oC under vacuum for one day. Aluminum cathode was deposited using thermal vacuum evaporation technique at $1x10^{-5}$ torr for one minute also. Five wires were connected to the electrodes using silver paste. The side view of the sample with anode and cathode is depicted in Figure (3.5). The film thickness of the organic film was measured using a calibrated homemade variable angle spectroscopic ellipsometer (VASE). Figure (3.6) depicts the experimental setup arrangement.

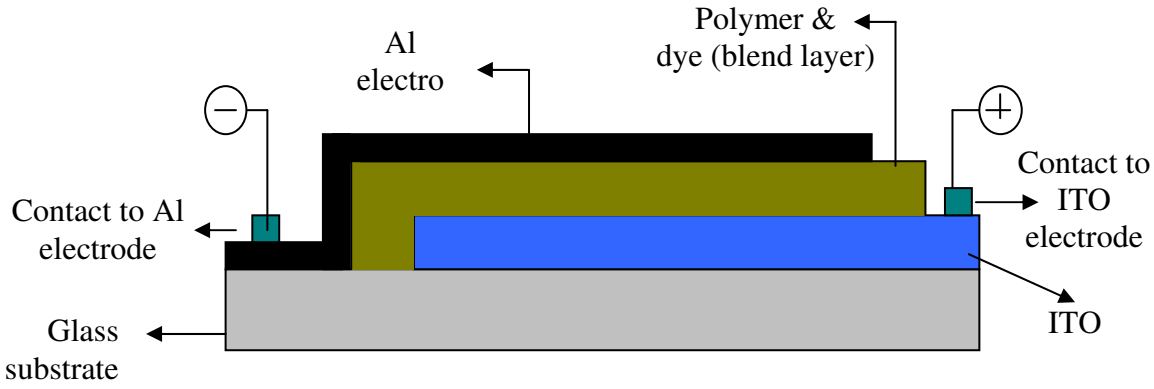

(a)

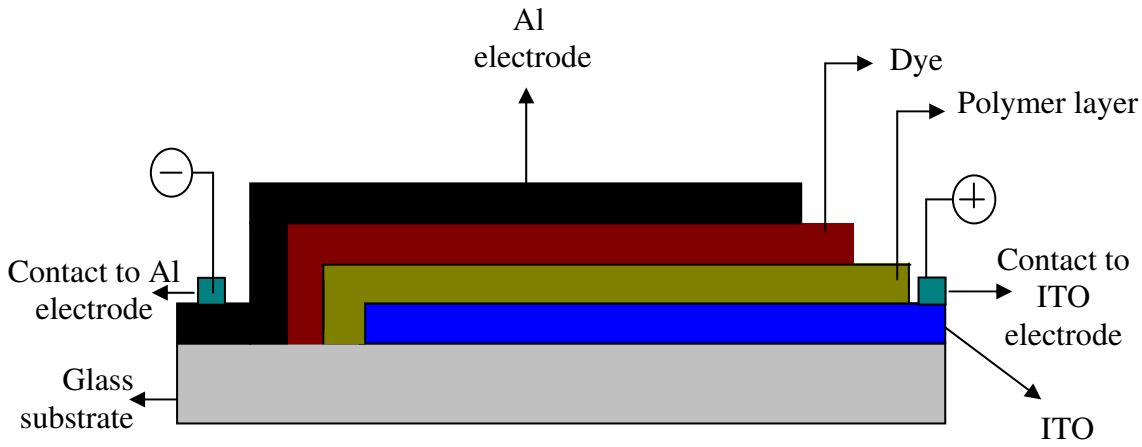

(b)

Figure (3.4) Typical structure of (a) a single layer OLED sample, and (b) a double layer OLED sample.

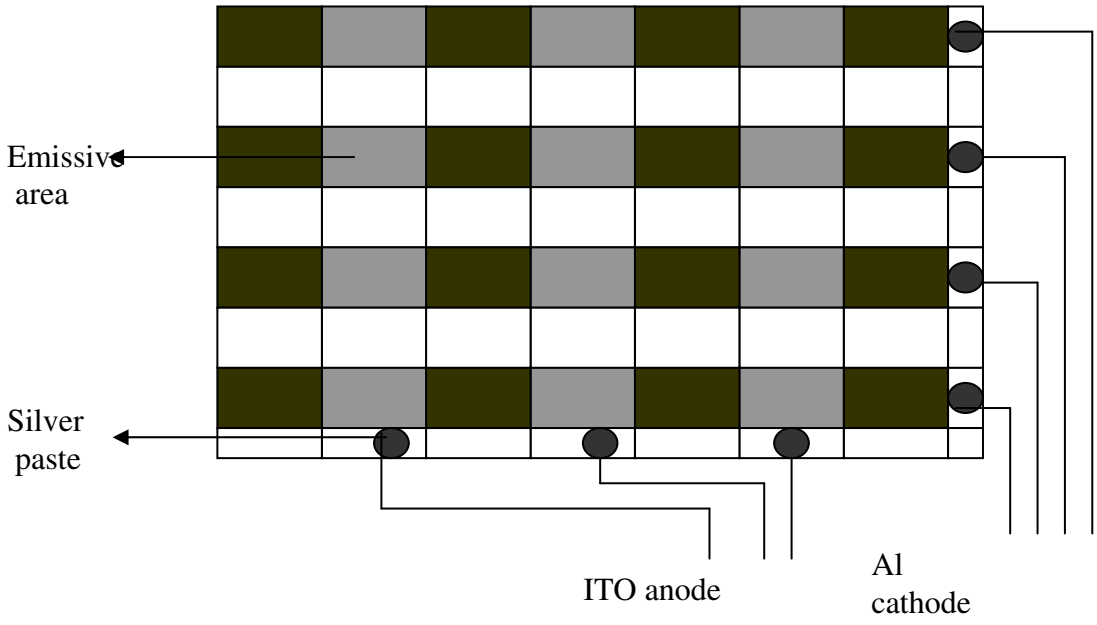

Figure (3.5) Top view of a sample with anode and cathode contacts shown.

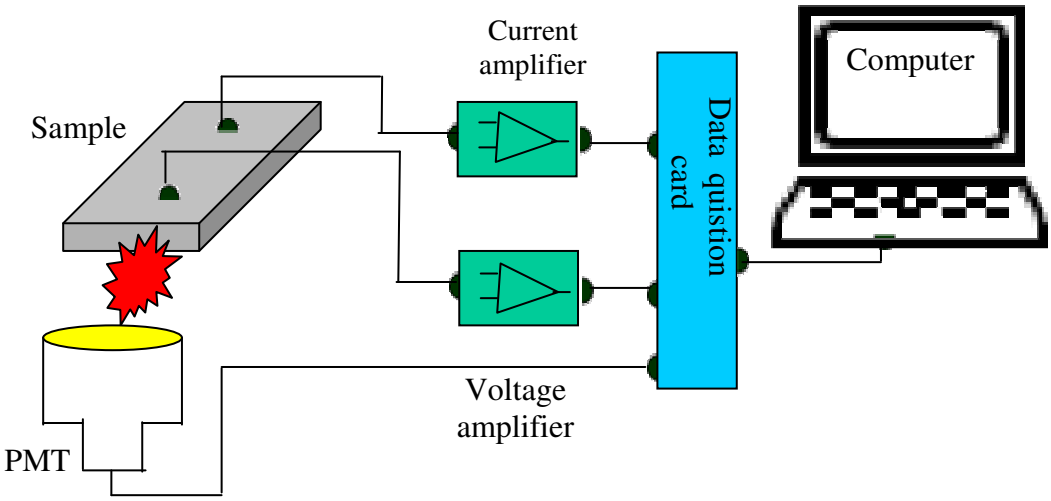

Figure (3.6) The experimental setup used in measurements.

3.4 Ellipsometry

3.4.1 Introduction

Ellipsometry is an optical sensitive technique for investigating the dielectric properties (refractive index N) and the thickness of thin films. It has applications in many fields such as semiconductors, electronics, optics, and industrial applications. An ellipsometer measures the changes of polarization state of light, when reflected from a sample. A conventional ellipsometer consists of a light source, a polarizer, an analyzer, and a detector. Figure (3.7) shows the components of an ellipsometer in common form [35,36, 37].

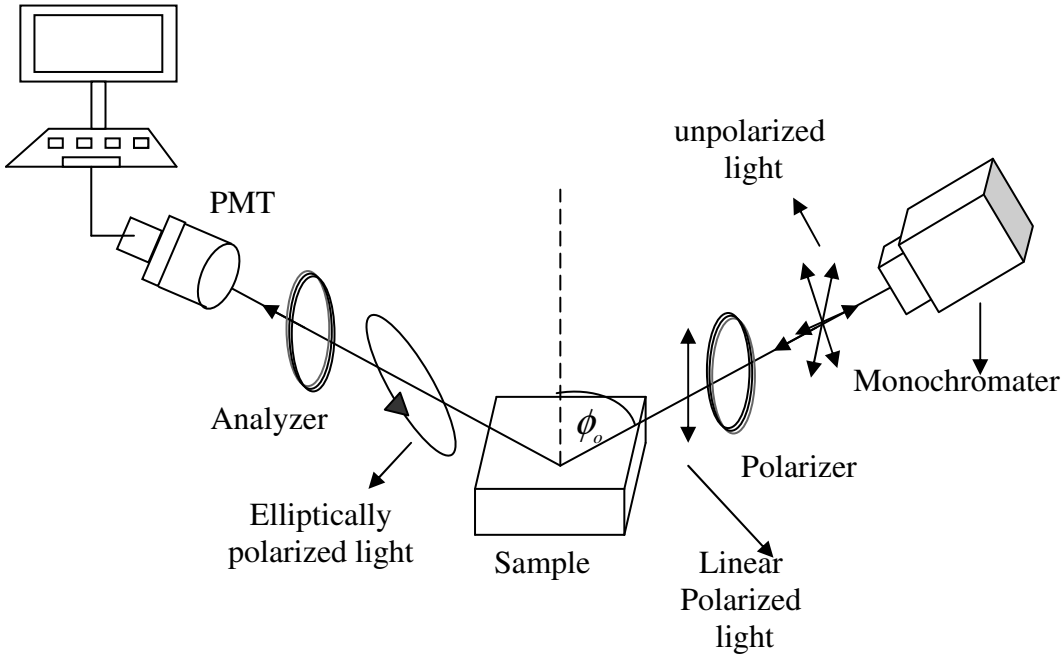

Figure (3.7) Ellipsometer in common form.

The principle of operation of an ellipsometer is illustrated by the schematic drawing of the ellipsometer in the Figure (3.7). The incident light is linearly polarized with finite electric field components E_p and E_s in the direction parallel and perpendicular to the plane of incidence respectively. Upon reflection, the polarization state of the S and P components of the electric field will change. The reflected light becomes elliptically polarized as shown in Figure (3.9) [38,39].

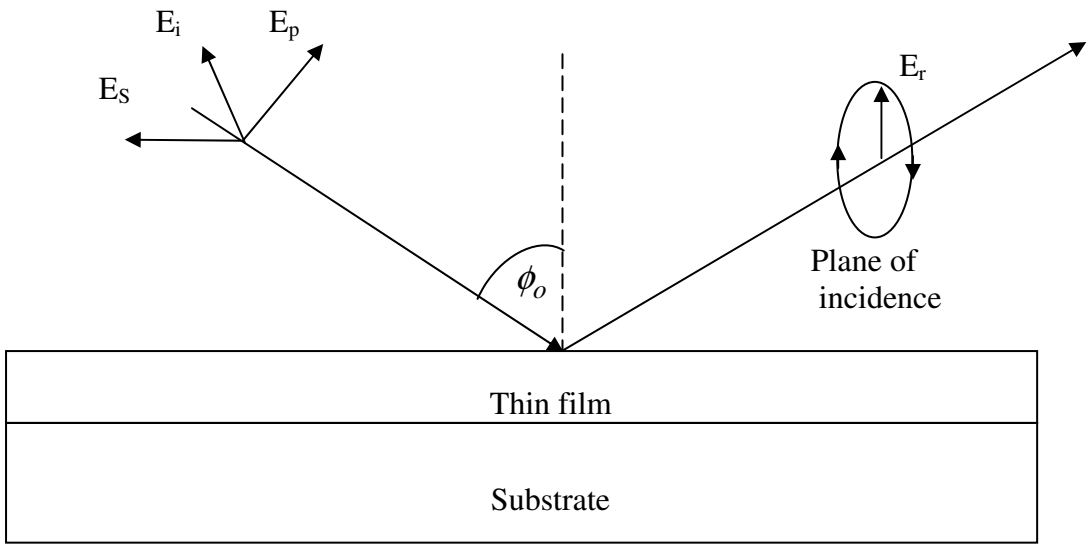

Figure (3.8) Schematic depiction of an ellipsometic set-up

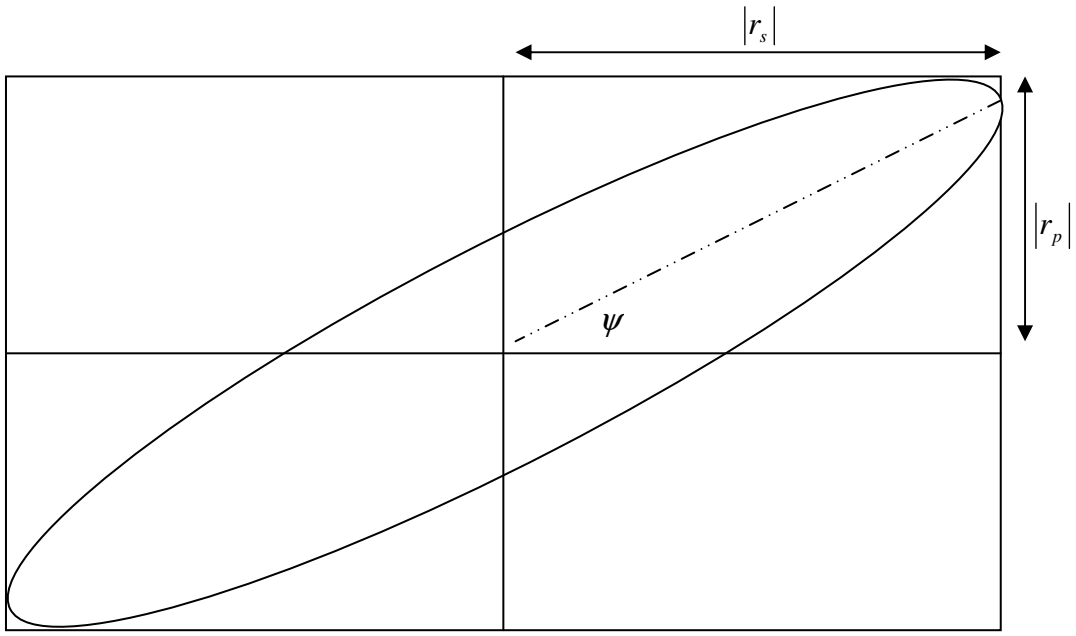

Figure (3.9) Geometry of the elliptically polarized light

Consider the reflected $P-$polarization δ_{rp} and the reflected $S-$polarization δ_{rs}. We can define the parameter Δ as

$$\Delta = \delta_{rp} - \delta_{rs} \tag{3.1}$$

which represents the change in phase difference that occurs upon reflection. It can has the value from 0^o to 360^o. The amplitudes of both the parallel and the perpendicular components r_p and r_s (see equations 3.10, 3.12) change upon reflection. The ratio of the absolute value of amplitudes of outgoing wave for the parallel component and the absolute value of amplitude of the outgoing wave for the perpendicular component is called $\tan\psi$ such that

$$\psi = \tan^{-1}\left(\frac{|r_p|}{|r_s|}\right) \tag{3.2}$$

Ellipsometer measures two values, the change in amplitude difference ψ, and the change in phase difference Δ.

These two values are related to the ratio of Fresnel's reflection coefficients, r_p and r_s for P and S components of polarized light, respectively. The ellipsometric parameters ψ and Δ can be directly inverted to give both real and imaginary parts of the complex refractive index, n and κ respectively. This can be done using the fundamental ellipsometric equation

$$\rho = \frac{r_p}{r_s} = \tan(\psi)e^{i\Delta} \tag{3.3}$$

where ρ is the complex ratio of the reflection coefficients

3.4.2 Typical Components of an Ellipsometer

(a) Light Source

An ellipsometer requires a light source laser or a lamp. Laser is intense and collimated beam with small spot size; however laser is considered as a single wavelength light source. This means that spectroscopic ellipsometry can not be studied using laser source. Therefore, spectroscopic ellipsometry requires a broad spectrum of wavelengths in order to achieve spectroscopic measurements.

(b) Monochromator

Monochromator is a Greek word, which means single color. It is an optical device that transmits selectable narrow band of wavelengths of light chosen from a wider range of wavelengths of light. Monochromators have wide usage in many optical systems such as ellipsometers and spectrophotometers.

(c) Polarizer/Analyzer

The most important optical element in making an ellipsometer is the polarizer. It is used in two different ways, polarizer and analyzer. A polarizer is a device that converts an unpolarized (mixed of polarized) light into a beam of defined polarization state. On the other hand, the analyzer is a polarizer that is used to convert elliptically polarized light into linearly polarized light or to determine the polarization state of the beam [38,39].

(d) Detectors

The purpose of the detector is to measure the intensity of light passing though the analyzer. A photomultiplier tube (PMT) is one of the most sensitive detectors, that allows to measure very low levels of light. It can detect ultraviolet, visible, and near infrared radiation. In general, every PMT has nine electrodes. Every electrode is called a dynode, which operates at a constant high voltage. A PMT consists mainly of light sensitive photo-cathode, that generates electrons when photons strikes the cathode. These electrons are directed to the positively biased dynodes. Every electron strikes the charged dynode creates several electrons, which are collected by the following dynode. The output of a PMT is converted to a current which depends on the intensity of light striking the photocathode [39].

3.4.3 Rotating Analyzer Ellipsometer (RAE)

RAE consists of a cascaded components of a light source, a polarizer, a sample, an analyzer, a detector, and a computer. In RAE, the polarizer is fixed, while the analyzer rotates continually during the measurements. The state of polarization before striking the sample is linear and is elliptical upon reflection. The polarization state of reflected light becomes linear after passing in the rotating analyzer. The

direction of polarization varies in time at the detector which measures the intensity as a function of time.

The PMT detects sinusoidally time dependent varying intensity I(t). It records different intensity at different states of polarization [40,41]. A Fourier analysis of the sine wave can be used to find the values of the ellipsometric parameters

$$I(t) = I_0[1 + \alpha\, x\cos(2\omega t) + \beta \sin(2\omega t)] \tag{3.4}$$

where, I_o is the average intensity, α, β are the Fourier coefficients of the intensity and ω is the angular frequency of the motor.

The Fourier coefficients of the intensity are related to the ellipsometric parameters ψ and Δ by

$$\alpha = \frac{\tan^2\psi - \tan^2 P}{\tan^2\psi + \tan^2 P} \tag{3.5}$$

$$\beta = \frac{2.\tan\psi.\cos\Delta.\tan P}{\tan^2\psi + \tan^2 P} \tag{3.6}$$

where P is the fixed polarizer angle

The ellipsometric parameters ψ and Δ can be written as

$$\tan\psi = \sqrt{\frac{1+\alpha}{1-\alpha}}\left|\tan P\right| \tag{3.7}$$

$$\cos\Delta = \frac{\beta}{\sqrt{1-\alpha^2}}\left(\frac{\left|\tan P\right|}{\tan P}\right) \tag{3.8}$$

After that, ψ and Δ can be inverted using statistical calculations to find the thickness and index of the thin film. Least –Square Approximation and quadratic equation methods are important methods used to calculate the thickness and the refractive index of thin films.

3.4.4 Reflection and Transmission by a Single Film

Consider a thin film of thickness d deposited on a substrate. A plane polarized beam is incident at the interface between the air (medium (0)) and the film (medium (1)), as shown in Figure (3.10). The light will suffer multiple reflections and transmissions. A phase difference is added when light travels between the upper and lower surfaces of thin film. It can be expressed by the following equation

$$\beta = 2\pi \frac{d}{\lambda} N_1 \cos(\phi_1) \tag{3.9}$$

where d is the thickness of the thin film, ϕ_1 is the angle of refraction, N_1 is the complex refractive index of the thin film, and λ is the wavelength of the incident light beam.

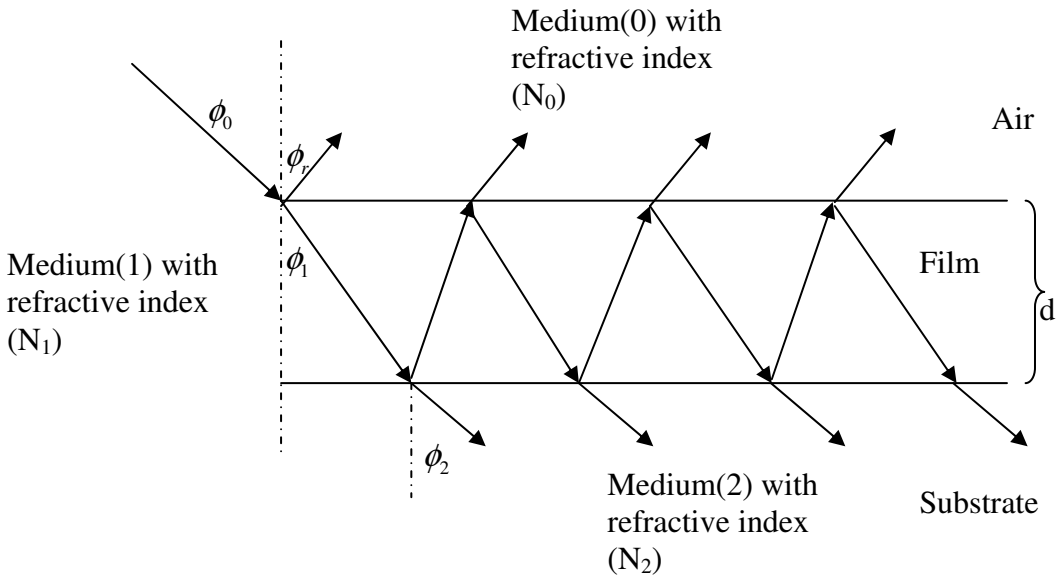

Figure (3.10) Multiple reflection and transmission by a thin film.

According to Figure (3.11), the complex Fresnel's reflection and transmission coefficients of this system are given by [38,40]

$$r_p = \frac{r_{01p} + r_{12p} \exp(i\beta)}{1 + r_{01p} r_{12p} \exp(i\beta)} \tag{3.10}$$

$$t_p = \frac{t_{01p} t_{12p} \exp(i\beta)}{1 + r_{01} r_{12p} \exp(i\beta)} \tag{3.11}$$

$$r_s = \frac{r_{01s} + r_{12s} \exp(i\beta)}{1 + r_{01s} r_{12s} \exp(i\beta)} \tag{3.12}$$

$$t_s = \frac{t_{01s} t_{12s} \exp(i\beta)}{1 + r_{01} r_{12s} \exp(i\beta)} \tag{3.13}$$

where r_p is the complex reflection coefficient for the P polarization, r_s is the complex reflection coefficient for the S polarization, t_p is the complex transmission coefficient for the P polarization and t_s is the complex transmission coefficient for the S polarization respectively. For more details see appendix (B).

3.4.5 Thickness and Index Calculations Using An Ellipsometer

(a) Quadratic Equation Method

Quadratic equation method was driven by Samuel S.So in 1976 [41]. By substituting Fresnel's coefficients r_p and r_s into equation (3.3), we get

$$\rho = \frac{\left(r_{01p} + r_{12p} e^{i\beta}\right)\left(1 + r_{01s} r_{12s} e^{i\beta}\right)}{\left(1 + r_{01p} r_{12p} e^{i\beta}\right)\left(r_{01s} + r_{12s} e^{i\beta}\right)} \tag{3.14}$$

$$(r_{12p} r_{12s} (r_{01p} - r_{01s})) e^{2i\beta} + (r_{01s} r_{01p} (\rho r_{12p} - r_{12s}) + \rho r_{12s} - r_{12p}) e^{i\beta} + (\rho r_{01s} - r_{01p}) = 0 \tag{3.15}$$

Assume that

$$\text{A} = \left(r_{12p} r_{12s} (r_{01p} - r_{01s})\right),$$

$$\text{B} = \left(r_{01s} r_{01p} (\rho r_{12p} - r_{12s}) + \rho r_{12s} - r_{12p}\right),$$

$$\text{C} = \left(\rho r_{01s} - r_{01p}\right),$$

and $\mathrm{T} = e^{i\beta}$

Then, equation (3.15) can be simplified to give a quadratic equation as

$$A\mathrm{T}^2 + BT + C = 0 \tag{3.16}$$

The solutions of quadratic equation have the next form

$$T = e^{i\beta} = \frac{-B \pm \sqrt{B^2 - 4AC}}{2A} \tag{3.17}$$

from equation (3. 9)

$$d = \frac{\lambda\beta}{\left(2\pi N_1 \cos(\phi_1)\right)} \tag{3.18}$$

Substituting from equation (3.17) into equation (3.18) the thickness of the film can be written in term of T, N_1 and ϕ_1 as

$$d = \frac{\lambda \ln T}{i\left(2\pi N_1 \cos(\phi_1)\right)} \tag{3.19}$$

(b) Least –Square Approximation

There are many methods used to determine the optical parameters of thin film. The common technique is the least square approximation. The principle of (least square approximation) is finding the smallest sum of the square of the differences between the ordinates of the function and the given point set. The main idea in this method is to minimize the difference between the calculated $(\psi_{calc}, \Delta_{calc})$ and the measured $(\psi_{\exp}, \Delta_{\exp})$ .The smallest the difference χ is the better fit. χ is given by

$$\chi^2 = \frac{1}{n-m-1}\sum_{i=1}^{n}\left[\frac{\psi_{icalc} - \psi_{i\exp}}{\delta_{\psi,i}^{\exp}}\right]^2 + \frac{1}{n-m-1}\sum_{i=1}^{n}\left[\frac{\Delta_{icalc} - \Delta_{i\exp}}{\delta_{\Delta,i}^{\exp}}\right]^2 \tag{3.20}$$

where n is the number of the experimental observation points, m is the number of fit parameters that completely characterized the sample under test, $\delta_{\psi,i}^{\exp}$ is the

measurement uncertainty of ψ and $\delta_{\Delta,i}^{\exp}$ is the measurement uncertainty of Δ [40]. A home Matlab subroutine was used to determine the refractive index and the thickness of the thin film of some samples.

3.5 Cauchy's Equation

Cauchy's equation is a solution of non-homogeneous second order differential wave equation in electromagnetic theory which is known as Lorentz model. Cauchy's equation is used to describe the normal dispersion of dielectric materials in the visible wavelength region. It is an empirical relationship between the refractive index and the wavelength of light which uses in transparent material.

$$n(\lambda) = A + \frac{B}{\lambda^2} + \frac{C}{\lambda^4} \tag{3.21}$$

where A, B and C are called Cauchy's constants. In some references Cauchy's constants may be written in term of (n_1, n_2, n_3), where (n_1, n_2, n_3) are three different values of refractive index in three different wavelengths, which are characteristic of transparent materials. To plot the Cauchy curve, it is necessary to find three different values of n for three different values of λ's. Cauchy constants can be determined for a transparent material by fitting the equation using suitable software program [42].

Chapter Four

Results and Discussion

4.1 Introduction

In this chapter, we present the results and discussion of our work on five different OLED samples. These results include the I-V characteristic curves, the dependence of light intensity on voltage and current, and the conduction mechanism. The organic material is Poly-(9-Vinylcarbazole) which acts as a hole transport layer, doped with various dyes (8-hydroxyquinoline aluminum (Alq_3), rhodamine 6G, 1,3,4-oxadiazole, carbocyanine, and fluroscein). The relative light intensity was measured using a PMT (photomultiplier tube) for all samples biased over the full range of voltages from 0 to 9 volts. Finally, additional ellipsometry measurements that include optical parameters of thin films will be reported. The data was recorded and saved as an ASCII file, analyzed and plotted using Origin 5.0 from Microcal Software, Inc. Electrical measurements where conducted at room temperature and in nitrogen chamber in order to prevent oxidation. The driving voltages and the currents were obtained and measured using a MetraByte's Das-20 data acquisition card interfaced with a personal computer. The output of the PMT was amplified then collected by the same data acquisition card.

4.2 Results and Discussion

Figure (4.1) through Figure (4.5) depict the various characteristics of the five samples under study. The current-voltage characteristics, relative light intensity-voltage characteristics, relative light intensity-current characteristics, and current-voltage in logarithmic scale are shown in these figures.

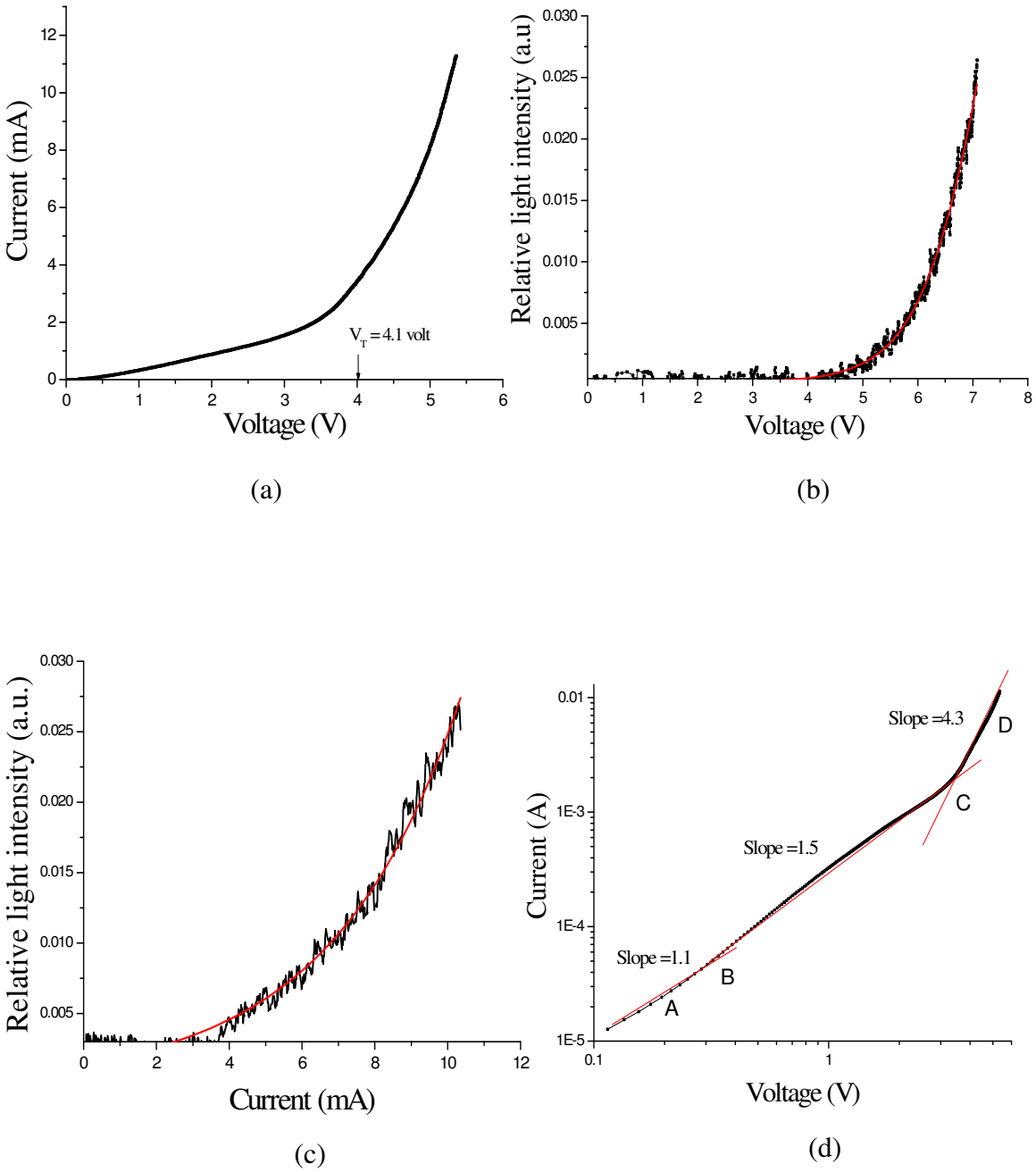

Figure (4.1) Four characteristics curves of S_1, (a) Current- voltage characteristics, (b) Relative light intensity-voltage characteristics, (c) Relative light intensity-current characteristics, (d) Current-voltage in logarithmic scale.

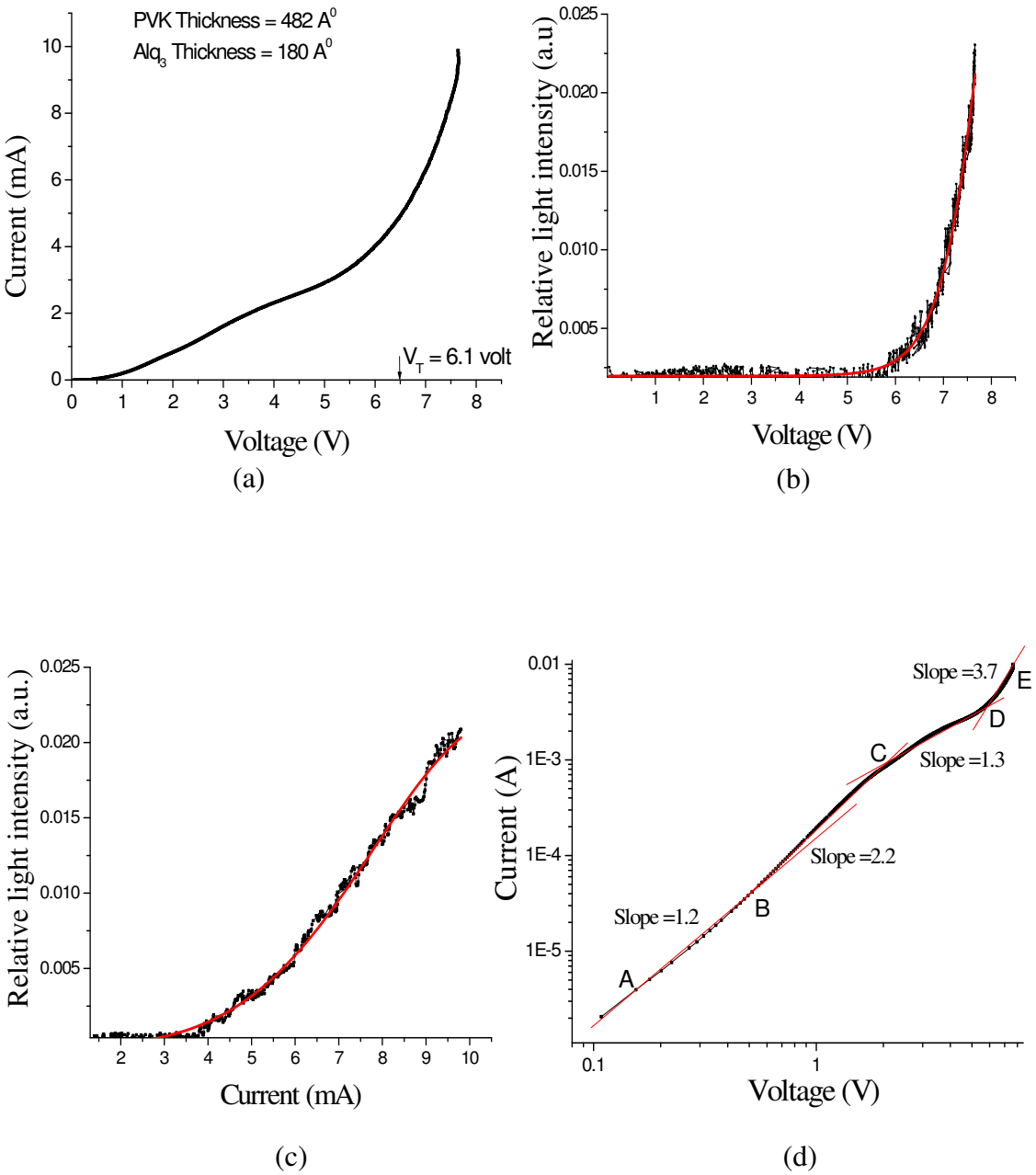

Figure (4.2) Four characteristics curves of S_2, (a) Current- voltage characteristics, (b) Relative light intensity-voltage characteristics, (c) Relative light intensity-current characteristics, (d) Current-voltage in logarithmic scale.

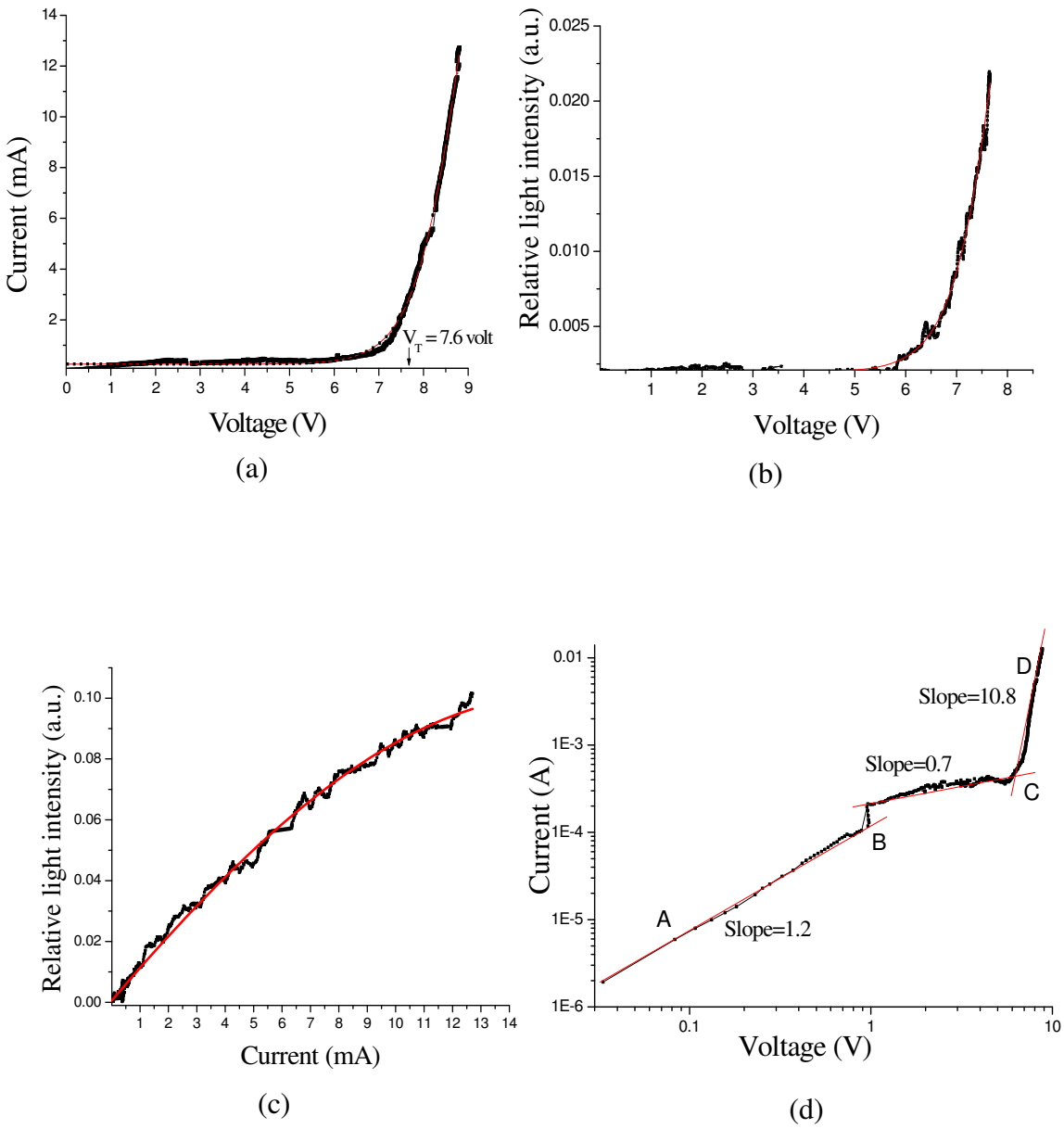

Figure (4.3) Four characteristics curves of S_3, (a) Current- voltage characteristics, (b) Relative light intensity-voltage characteristics, (c) Relative light intensity-current characteristics, (d) Current-voltage in logarithmic scale.

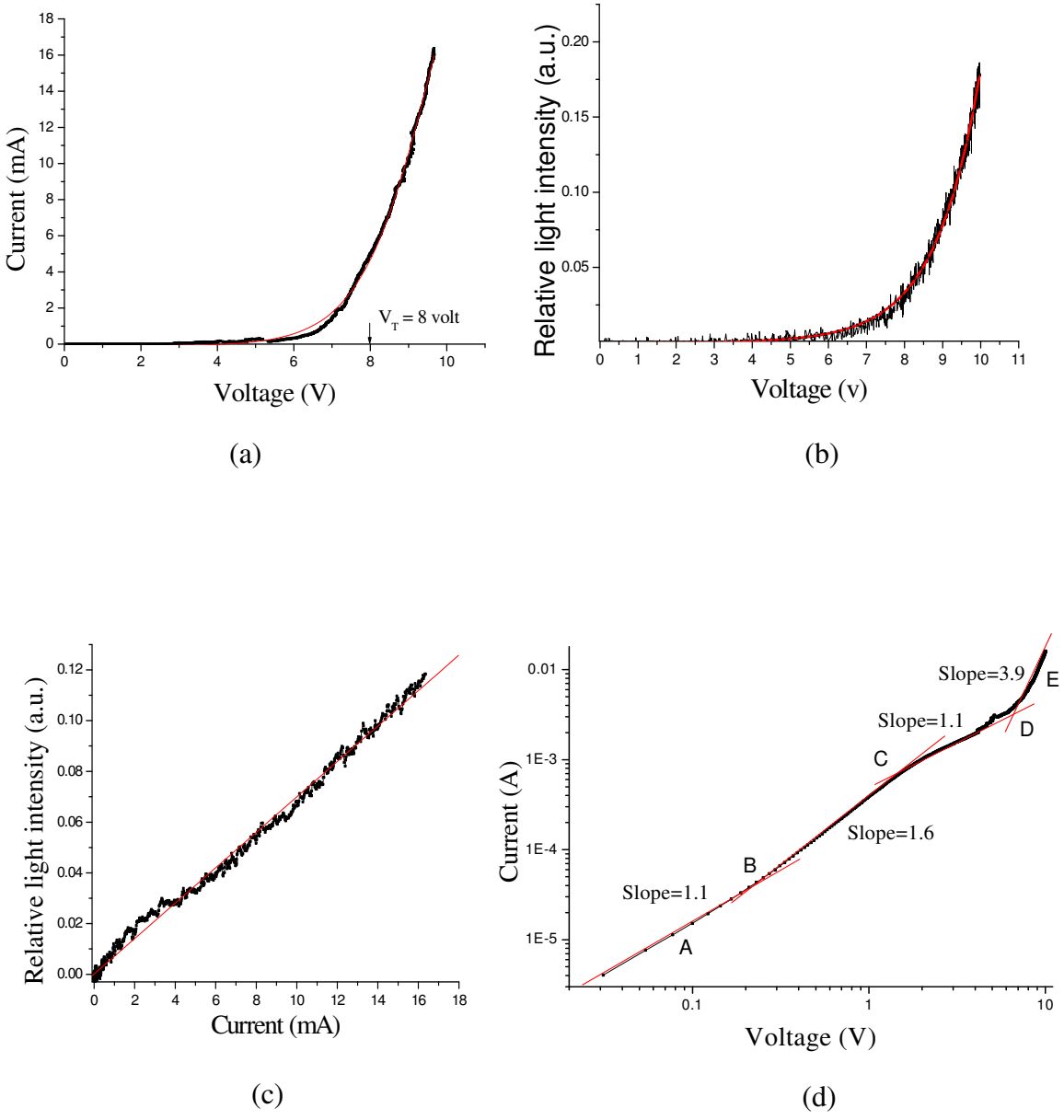

Figure (4.4) Four characteristics curves of S_4, (a) Current- voltage characteristics, (b) Relative light intensity-voltage characteristics, (c) Relative light intensity-current characteristics, (d) Current-voltage in logarithmic scale.

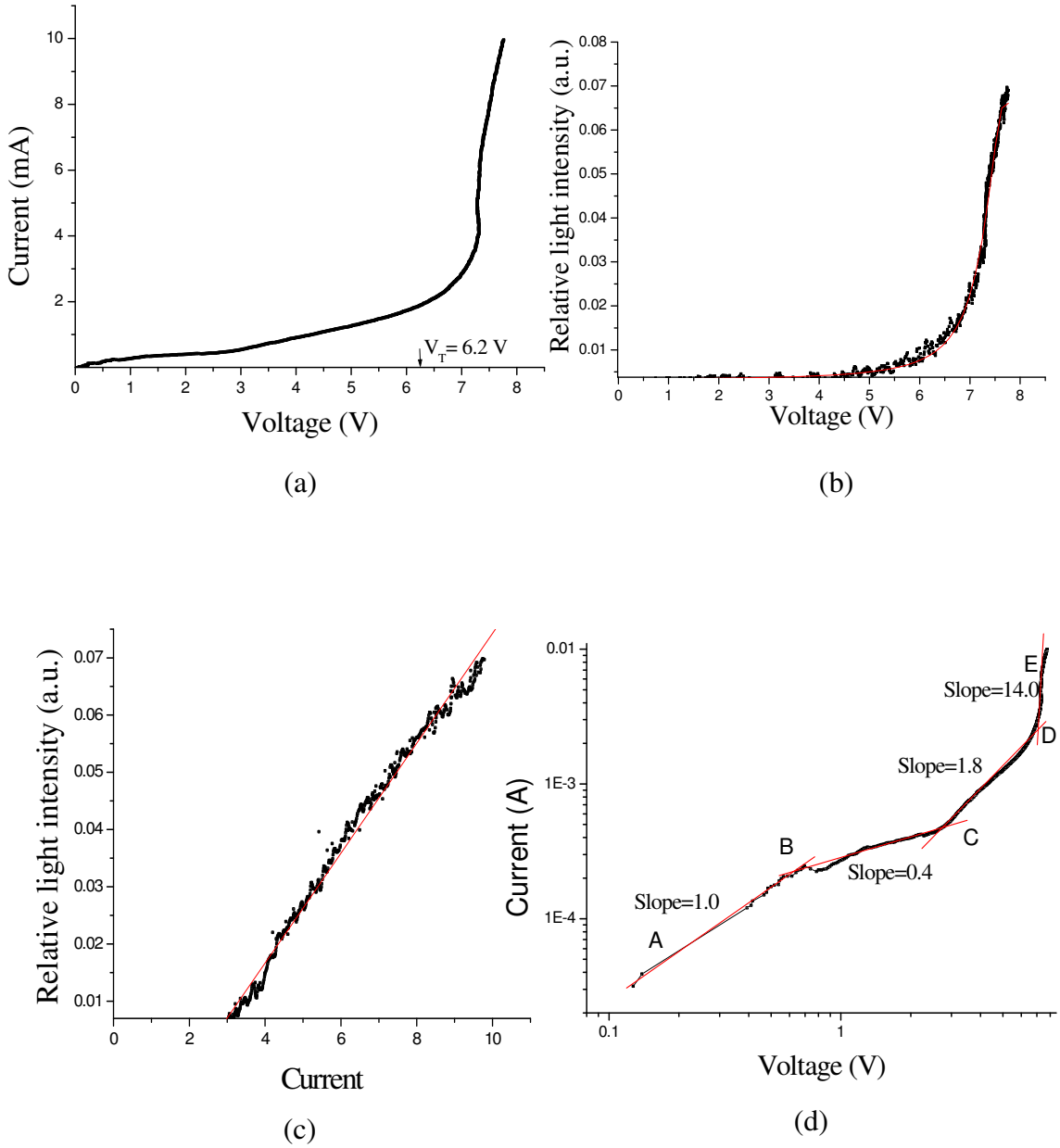

Figure (4.5) Four characteristics curves of S_5, (a) Current- voltage characteristics, (b) Relative light intensity-voltage characteristics, (c) Relative light intensity-current characteristics, (d) Current-voltage in logarithmic scale.

4.2.1 DC I-V Characteristic Curves

The forward bias was obtained when the transparent electrode was positively biased and the aluminum electrode was negatively biased. The non-linearity is frequent in I-V characteristics for all samples. The current passing through a sample is due to the injection of the charges from the electrodes. A comparison between the current-voltage characteristics of the these samples from sample1 through sample5 (S_1, S_2, S_3, S_4 and S_5) is depicted in Figure (4.6). DC I-V plots have been shown to be useful in establishing the current transport physics of OLED samples. These I-V characteristics show an exponential increase of current with the applied voltage, which is similar to a typical diode characteristic curve [43]. Under forward DC bias, the current increases slowly with increasing of voltage. Threshold voltage, V_T, is an important parameter characterizing the operation of OLEDs. In general it is the voltage at which the OLED begins to emits light. At certain higher voltage, which is the threshold voltage, the current increases sharply. The threshold voltages V_T were estimated by linearly extrapolating the I-V curves back to the voltage axis [44]. The curves represent S_3 and S_4 show a slow increase of the current at lower voltage, however in samples S_1, S_2 and S_5 , remarkable increase in current at the same voltage. I-V curves of the five OLED samples can be classified into two sets.

In set one, which includes S_1, S_2 and S_5. The current clearly appears at low applied voltage, however in set two which includes S_3 and S_4, the current appears at higher voltage. The sharp increase at low voltage in S_1, S_2 and S_5 may be referred to the leakage current, which is linearly dependent on the applied voltage. The leakage current observed properly due to movement of Al atoms inside the organic layer toward the ITO electrode. The movement of Al atoms towards the other electrode will increase the leakage current. This leads to low brightness of the OLED sample [45,46]. Back to the Figure (4.6), it was found that V_T of about 4.1V, 6.1 V and 6.2 V for S_1, S_2, and S_5, respectively.

In set two which includes S_3 and S_4, the leakage current is not appear evidently and V_T takes larger values, between (7.6 and 8 volt). In general the values of V_T are lower than the values of V_T reported for conventional organic light emitting

diode [46]. In general, the values of V_T for all samples are located between (4.0 and 8 volt). These values from I-V curves are reported in table (4.1).

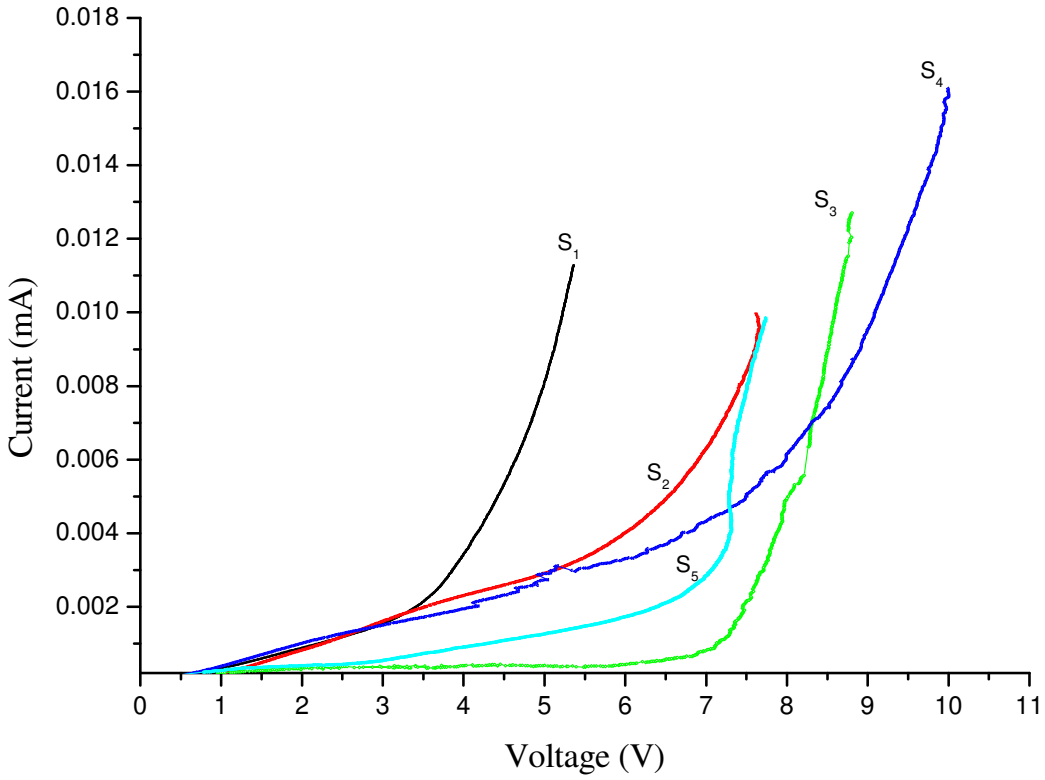

Figure (4.6) The current voltage characteristics of the S_1, S_2, S_3, S_4 and S_5 samples.

Table (4.1) Experimental values of threshold voltage for five samples

OLED sample	**S_1**	**S_2**	**S_3**	**S_4**	**S_5**
V_T (volt)	4.1	6.1	7.6	8.0	6.2

4.2.2 Variation of Relative Light Intensity with the Driving Voltage

The variation of the electroluminescence EL versus applied DC voltage of the five samples is depicted in Figure (4.7). It is clear from the Figure that the EL increases with increasing the forward bias voltage. At low voltages no EL is emitted. At certain higher voltage threshold voltage V_T, EL starts to emit. The EL can be clearly observed by the naked eye in dark environment, when the applied voltage exceeds V_T. The improved performance of S_3 and S_4 over that of other samples(S_1, S_2 and S_5) is clearly observed in Figure (4.7). The reason for this improved performance maybe referred to the better balance in the number of injected holes and electrons in emissive layers in the S_3 and S_4 samples compared to other samples.

The sample S_1 exhibits EL at 4.1 V, and maximum brightness is achieved at an operating voltage of 5.5 V while the sample S_4 exhibits EL at 8 V and maximum brightness is achieved at an operating voltage of 10 V. In general, the emitted EL becomes detectable at almost the same bias as these obtained from I-V characteristics measurements. It is clear from Figure (4.7) that sample S_4 exhibits the highest value of the electroluminescence at the operating voltage nearly 10 volt.

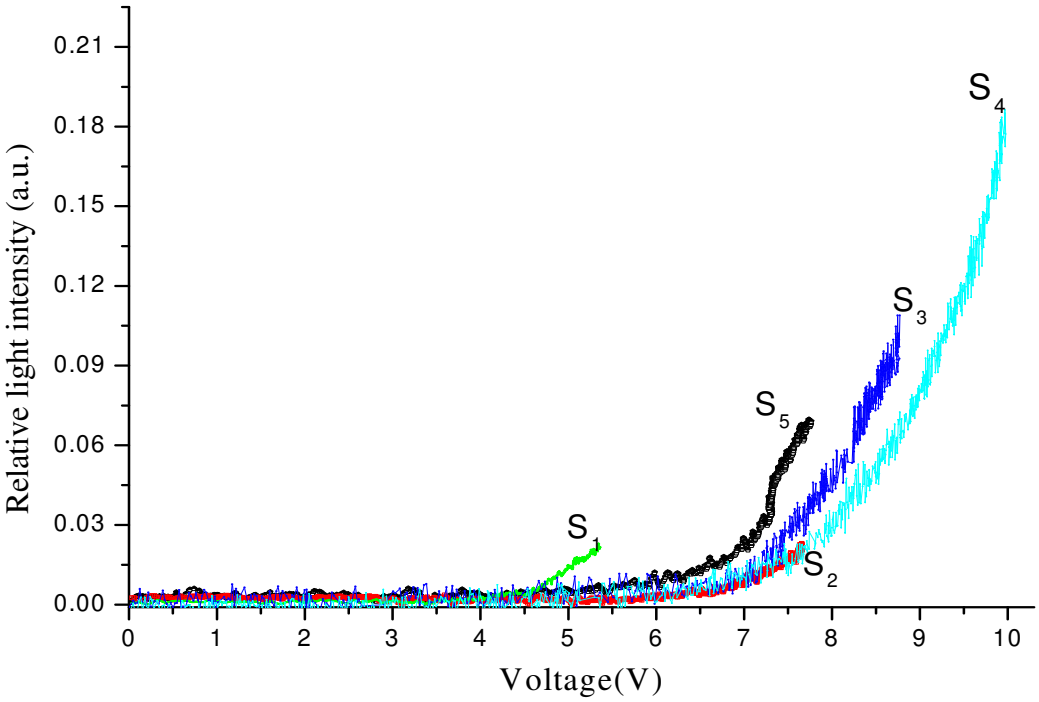

Figure (4.7) Electroluminescence-voltage characteristics of the S_1, S_2, S_3, S_4 and S_5 samples.

4.2.3 Variation of Relative Light Intensity with Increasing the Current

Figure(4.8) illustrates that the variation of the electroluminescence EL with current. It is clear that some samples exhibit linear growth relationships between EL and current, as reported in literature for OLEDs with spin coating deposition [47]. It also shows that the leakage current clearly appears in S_1, S_2 and S_5 samples. The largest leakage current occurs in S_2 sample equal to 5.4 mA. On the other hand, the leakage currents in the S_1 and S_5 samples are 3.8 mA and 2.9 mA, respectively.

Dramatic increases of sample S_5 relative light intensity exhibits at 3 mA, and then the relation between relative light intensity and current becomes linear relationship.

At low currents passing through the samples S_1 and S_2 there is no increase in relative light intensity. However, at higher currents, the rate of relative light intensity is higher than that at lower currents. Samples S_1 and S_2 exhibit that, the relative light intensities increase sharply with increasing injected current at 4mA and 5mA respectively. It is clear from Figure (4.8). that the leakage current becomes visible in the low parts of (S_1, S_2, S_5).

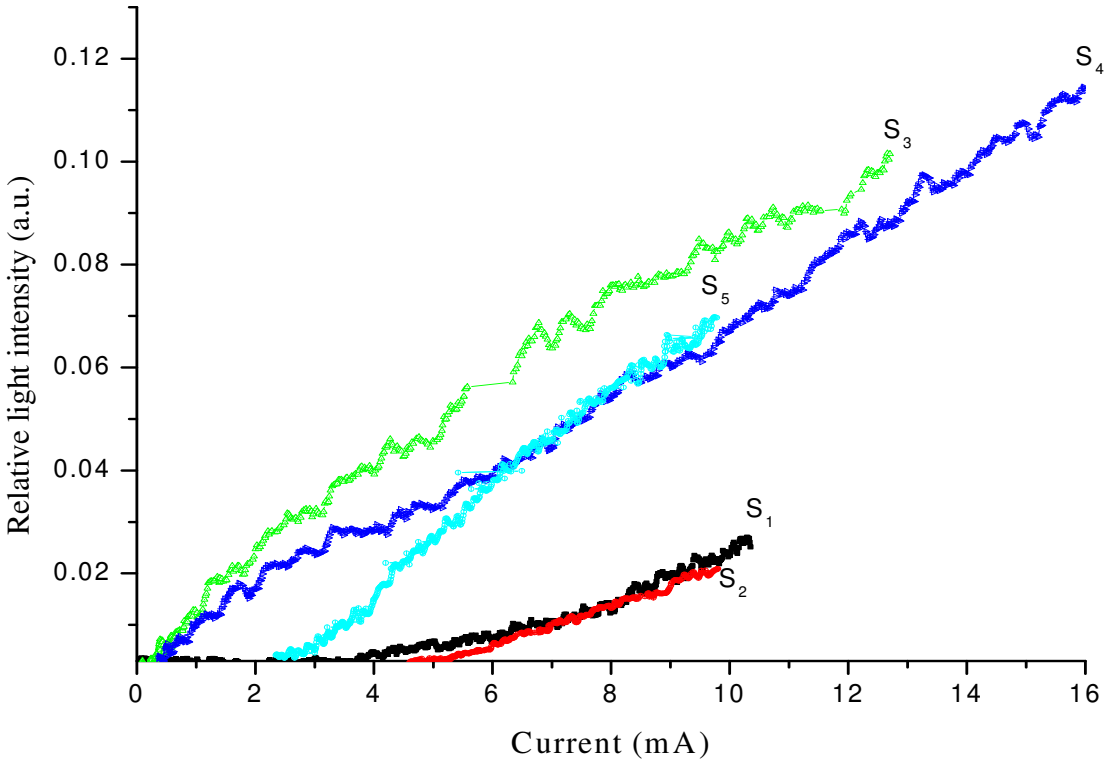

Figure (4.8) The variation of Electroluminescence with current.

4.2.4 Conduction Mechanism

Figure (4.9) shows the dependence of the current I on the voltage V in the natural logarithmic scale. Three (or four) regions can be seen in the current-voltage curve. These curves exhibit non-linear relationship. It is seen that the characteristics are distributed in three regions (marked AB, BC, and CD) as shown in samples S_1 and S_3. Four regions (marked AB, BC, CD, and DE) as shown in samples S_2, S_4 and S_5, which depicted in Figure (4.9). [31]. These different regions have different slopes which implies that the I-V relation (in the natural logarithmic scale) in type $I \alpha V^m$ where m is the slope of curve. Ohmic conduction at low voltage and space charge limited current SCLC at higher voltage can be expected from Figure (4.9).

In the first region (curves AB), slopes of all samples for region (AB) approximately equal unity, indicating that the conduction mechanism is ohmic. This also means that at very low voltages the current is directly proportional to the applied voltage. Beyond the ohmic region to the electroluminescence threshold, the dependence of the current on the voltage follows a power low ($I \alpha V^m$). In ohmic conduction the sample behaves as a large resistor. This mechanism is probably due to the density of majority carriers (electrons) injected into the organic layer is negligible in comparison to thermally generated charge carriers. In this case the current density J_{ohm} is given by

$$J_{ohm} = nq\mu_q \frac{V}{d} \tag{4.1}$$

where q is the electronic charge, μ_q is the electron mobility, V is the applied voltage, and d is the thickness of polymer layer [48].

Table (4.2) shows that S_2 has the largest slope in (BC) region which has a value nearly equal 2.2, and the lowest slop appear in S_5 which has a value nearly equal 0.4 for the same region. For the other samples of the same region, the slope varies between 0.7 and 1.6.

In the third region (CD) for S_5 the slope approaches to 2 which indicates that the current I depends quadratically on the voltage V. This behavior is a characteristic for space charge limited current (SCLC) in which J_{SCLC} is given by

$$J_{SCLC} = \frac{9}{8}\varepsilon\mu\frac{V^2}{d^3}. \tag{4.2}$$

SCLC of S_5 in (CD) region can occur if at least one electrode (Al or ITO) layer is able to inject more carriers than the material has in thermal equilibrium without carrier injection [31,48]. This means the thermally generated charge contribution is negligible. However, the lowest slope for S_4 is about 1.1, this means the conduction is ohmic at this region of S_4, but the largest slope is nearly equal 10.3 for S_3.

In the fourth region (DE), after the traps are filled, the current increases and the slope increases to the higher value [31]. All values of the slope for each reigns are tabulated in table (4.2).

Table (4.2) Experimental values of slope for each region of current-voltage of the five OLED samples in logarithmic scale

The slope	**S_1**	**S_2**	**S_3**	**S_4**	**S_5**
A-B	1.1	1.2	1.2	1.1	1.0
B-C	1.5	2.2	0.7	1.6	0.4
C-D	4.3	1.3	10.8	1.1	1.8
D-E	——	3.7	——	3.9	14.0

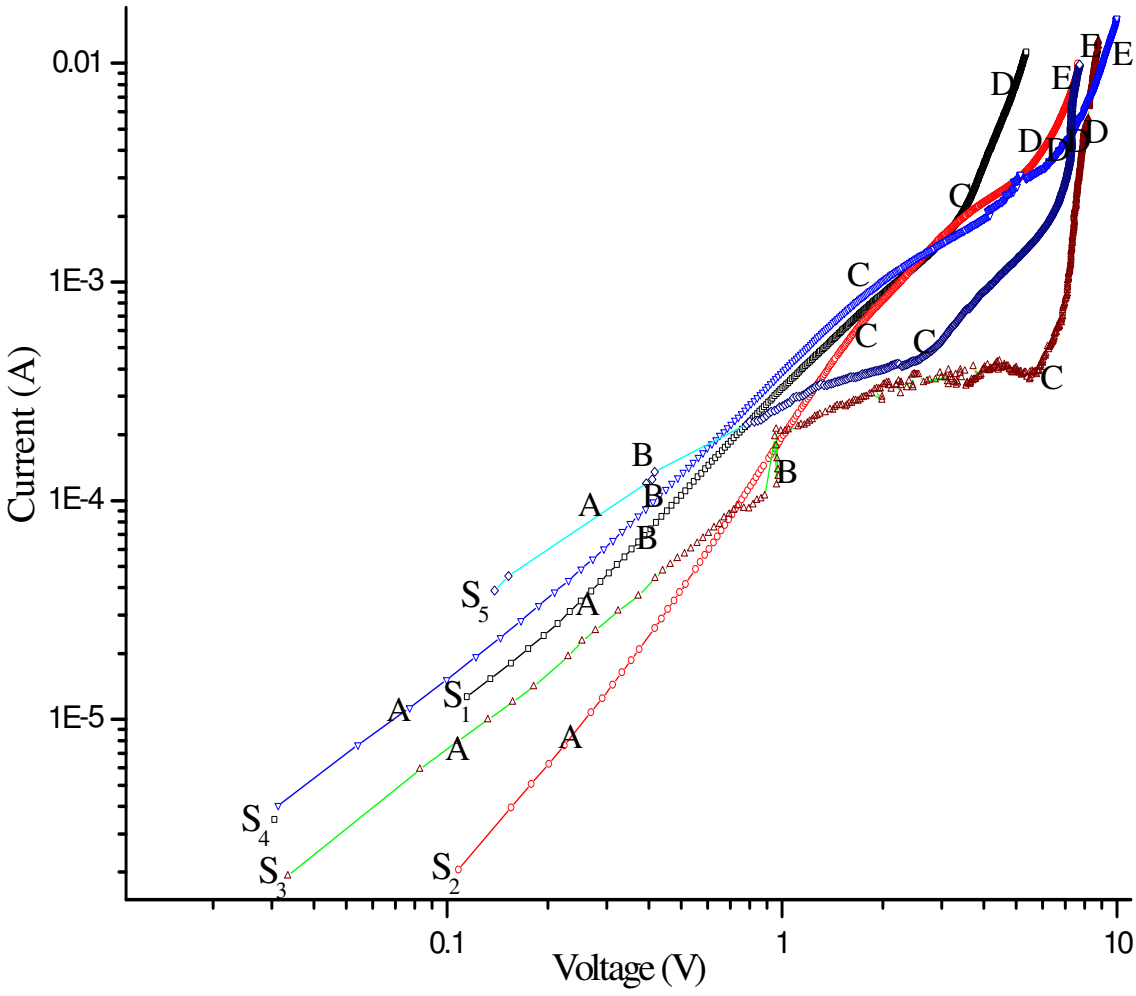

Figure (4.9) Current-voltage of the five OLED samples in logarithmic scale

4.3 Ellipsometry Measurements

4.3.1 Thickness and Refractive Index Determination

Ellipsometric data were taken at an angle of incidence equal to 75^o at room temperature. The data were analyzed and plotted using Origin 5.0 from Microcal Software, Inc. These curves include the variation of the real part of refractive index of (Alq_3 and PVK) thin films with visible spectrum of wavelengths, the variation of the change in amplitude difference Ψ with respect to the wavelengths λ, the variation of the change in phase difference Δ with respect to the wavelength λ and the relation between the change in phase difference Δ with respect to the change in amplitude difference Ψ.

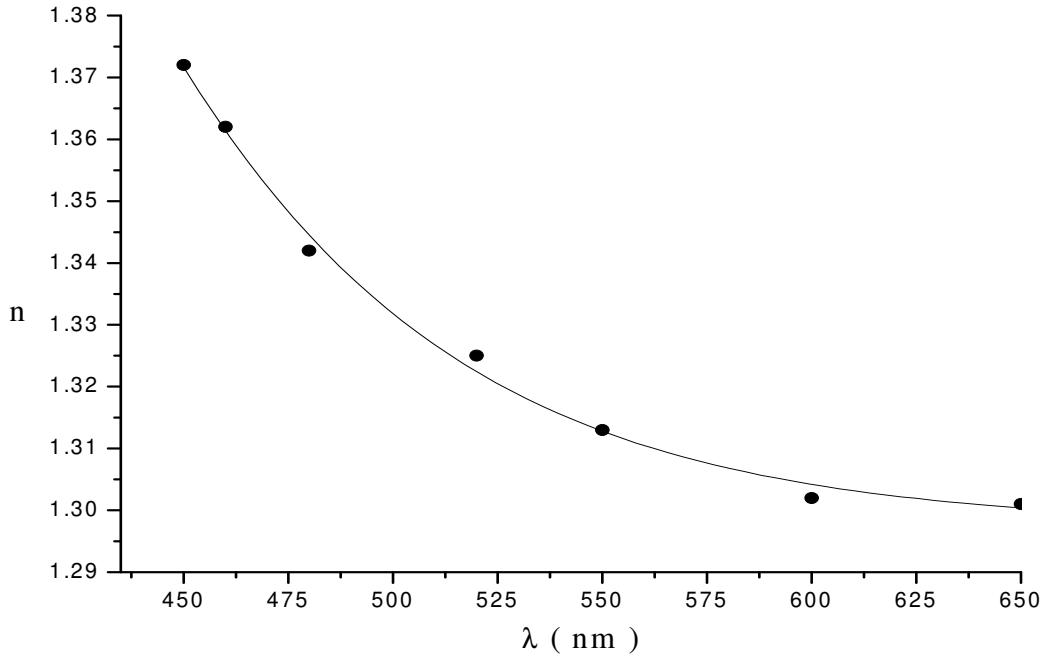

Figure (4.10) Variation of the refractive index of a 18 nm Alq_3 film on Si substrate with wavelength (visible spectrum) at 75^o angle of incidence

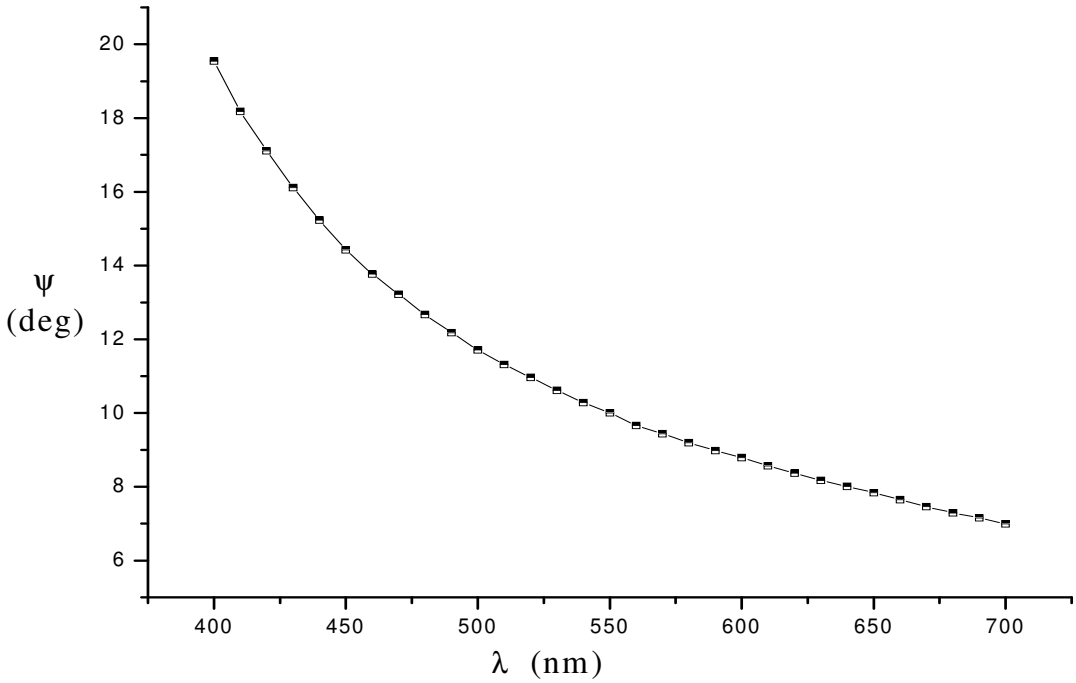

Figure (4.11) Psi as a function of λ from 400 to 700 nm for 18 nm Alq_3 film on Si wafer at 75° angle of incidence.

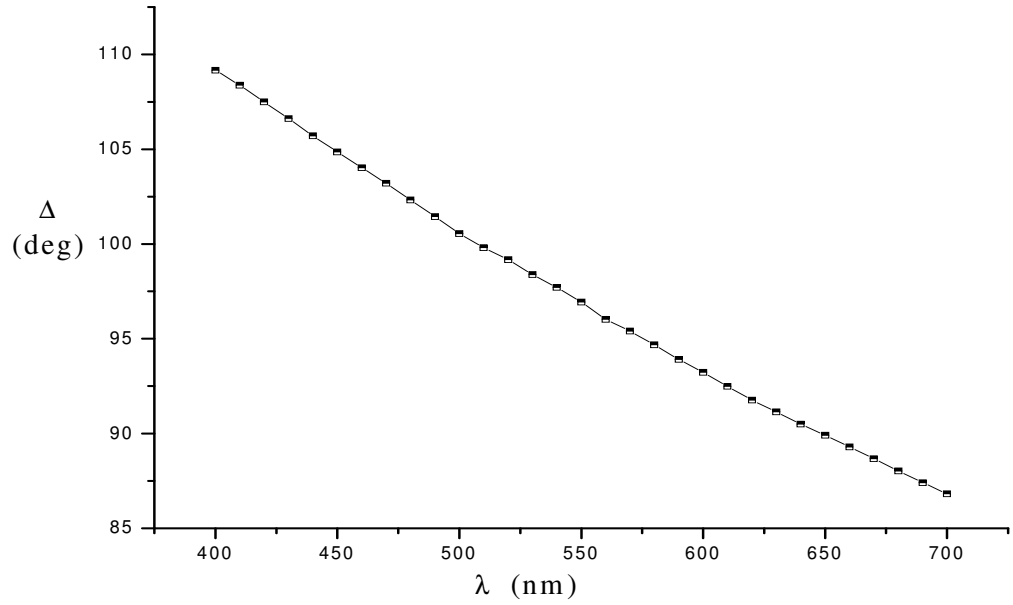

Figure (4.12) Delta as a function of λ from 400 to 700 nm for 18 nm Alq_3 film on Si wafer at 75° angle of incidence.

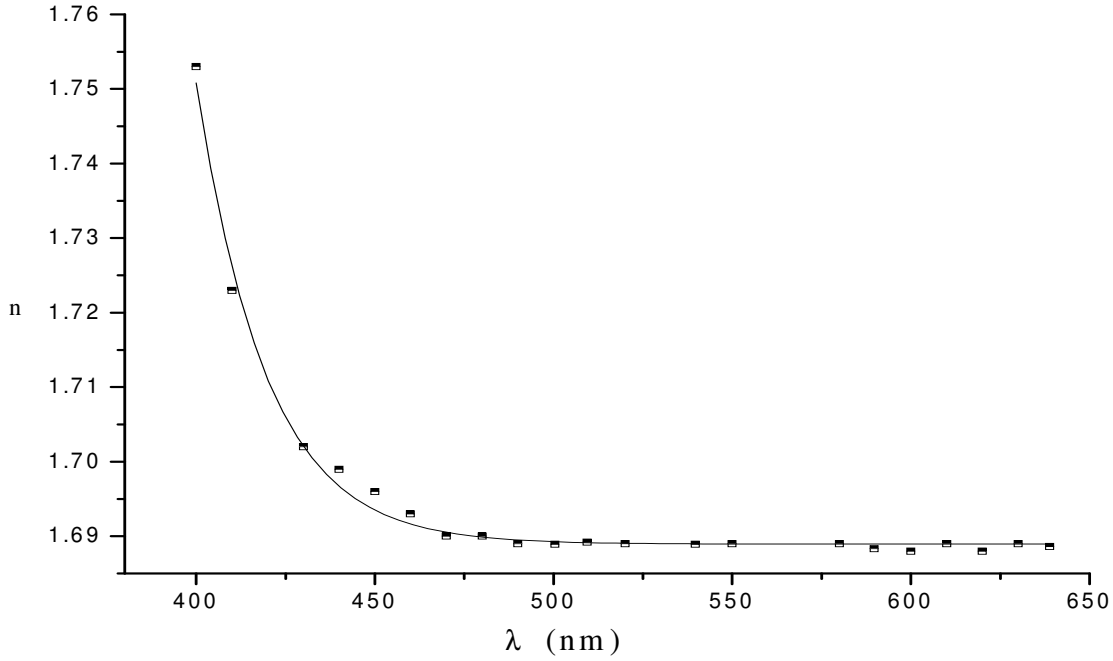

Figure (4.13) Variation of the refractive index of 48 nm PVK film on Si wafer with wavelength (visible spectrum) at 75^{o} angle of incidence

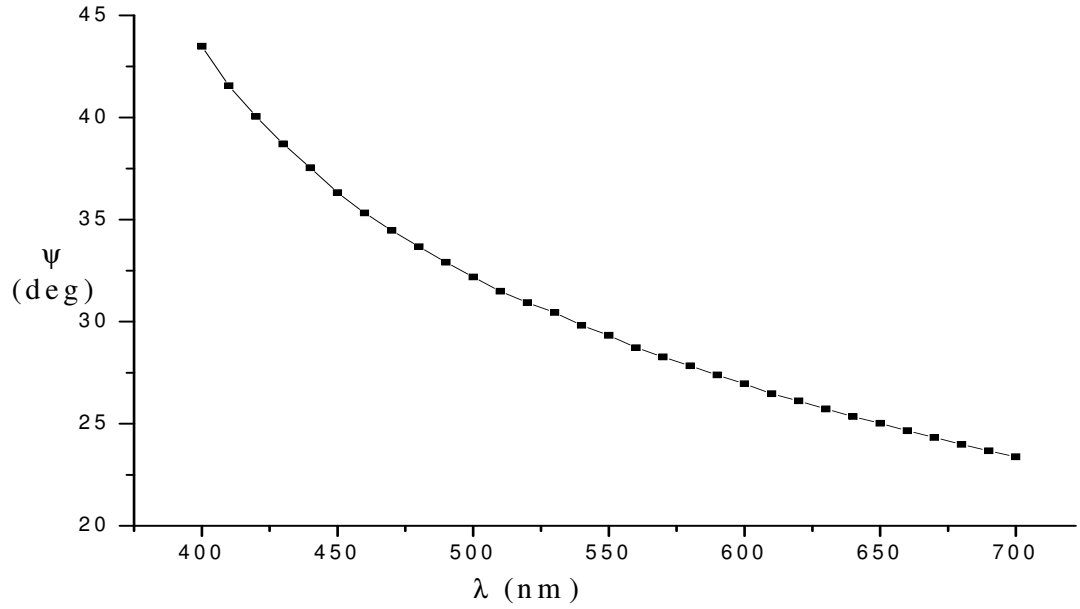

Figure (4.14) Psi as a function of λ from 400 to 700 nm for 48 nm PVK film on Si wafer at 75^{o} angle of incidence.

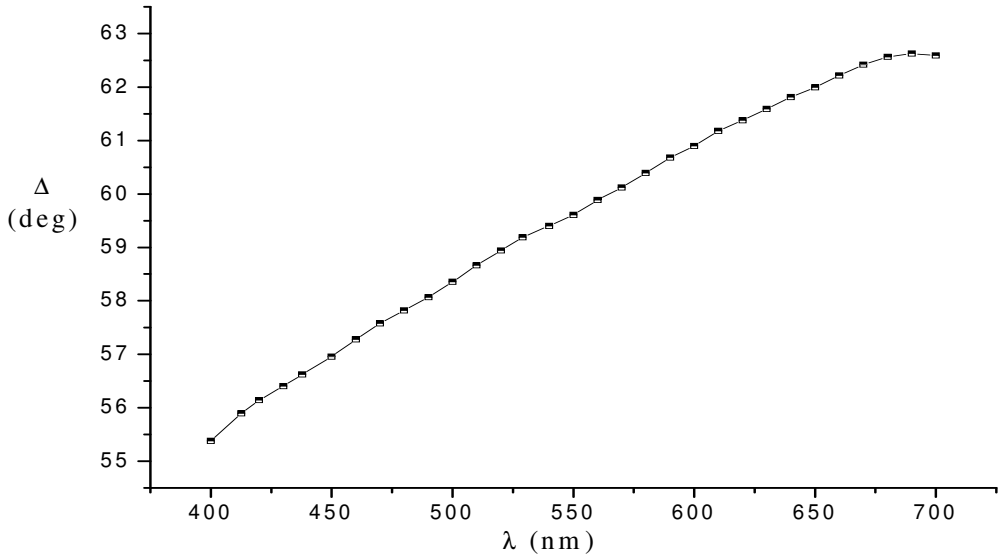

Figure (4.15) Delta as a function of λ from 400 to 700 nm for 48 nm PVK film on Si wafer at 75^{o} angle of incidence.

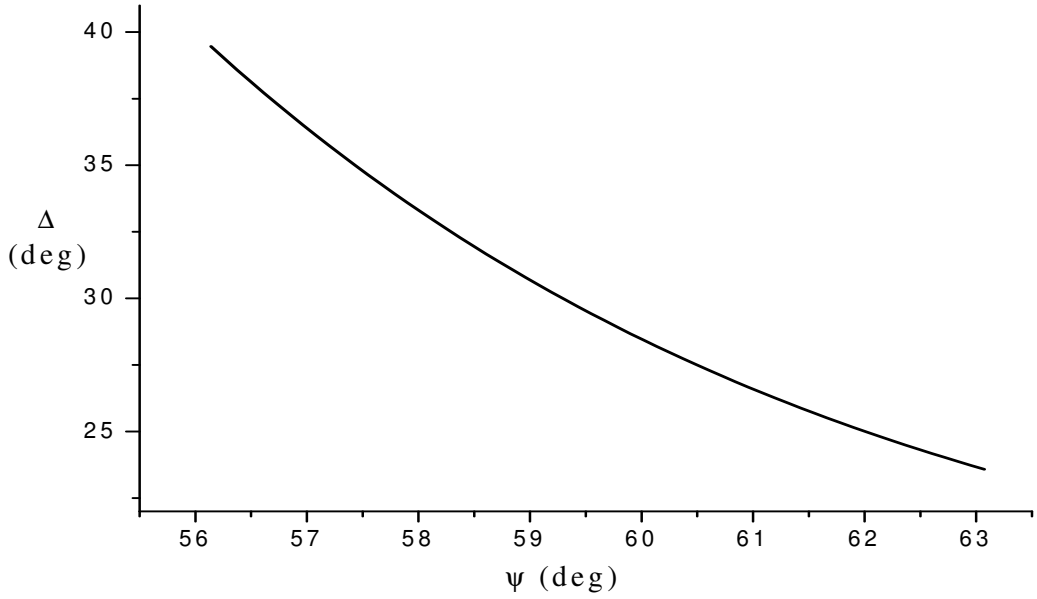

Figure (4.16) Delta-Psi for 48 nm PVK film on Si wafer at 75^{o} angle of incidence.

4.3.2 The Optical Parameters of Thin Films

We used a homemade variable angle spectroscopic ellipsometer VASE at 75° angle of incidence, at room temperature. Refractive index for Alq_3, PVK and the thickness can be calculated using VASE technique. The following equation is an equation which describes the behavior of refractive index as a function of wavelength λ. It is known as Cauchy's equation (see section 3.3.5).

$$n(\lambda) = A + \frac{B}{\lambda^2} + \frac{C}{\lambda^4} \tag{4.3}$$

where A, B and C are called Cauchy's constants.

Table 4.3. The values of A, B, and C in Cauchy relation for Alq_3 film on Si wafer and PVK film on Si wafer.

Sample	A	B	C
Alq_3 film on Si wafer	1.339	-0.3739×10^{7}	0.8915×10^{14}
PVK film on Si wafer	1.753	-0.416×10^{7}	0.6267×10^{14}

(a) Cauchy relation of a Alq_3 film (18 nm) on Si wafer with wavelength (visible spectrum) at 75° angle of incidence

$$n(\lambda) = 1.339 - \frac{0.3739\times10^{7}}{\lambda^2} + \frac{0.8915\times10^{14}}{\lambda^4}$$

(b) Cauchy relation of a PVK film (48 nm) on Si wafer with wavelength (visible spectrum) at 75° angle of incidence.

$$n(\lambda) = 1.753 - \frac{0.416\times10^{7}}{\lambda^2} + \frac{0.6267\times10^{14}}{\lambda^4}$$

CONCLOUSION

In this work, we conducted several measurements on five sets of samples (S_1 through S_5) with different structure and composition as described in section 3.3.1. Among these measurements are DC I-V characteristics of Poly(9-vinylcarbazole) film doped with different dyes, the variation of relative intensity with increasing the current and variation of relative intensity with the driving voltage. All electrical measurements were conducted at room temperature and in nitrogen chamber in order to prevent oxidation.

These I-V curves show an exponential increase of current with the applied voltage, which is similar to a typical diode characteristics. The smallest value of threshold voltage V_T was in (ITO/PVK R6G (blend)/Al) sample and the largest value was in (ITO/PVK 1,2,4 oxadiazole(blend)/Al) sample (see table (4.1)). In general the values of V_T are lower than the values of V_T reported for conventional organic light emitting diode.

It was found that the sharp increase of current clearly appears at low applied voltage in (ITO/PVK R6G (blend)/Al), (ITO/PVK/Alq_3/Al) and (ITO/PVK fluroscein (blend)/Al) samples. The sharp increase may be referred to the leakage current. In (ITO/PVK carbocyanine(blend)/Al) and (ITO/PVK 1,2,4 oxadiazole(blend)/Al) samples, the current appears at higher voltage.

We found that, at low applied voltage, the current is directly proportional to the applied voltage, this means that the conduction mechanism is ohmic. The current density –voltage dependence was found to obey the following relation,

$$J_{ohm} = nq\mu\frac{V}{d}$$

At higher applied voltage, we found that the current depends quadratically on the voltage in most samples. This indicated that the conduction in these films obeys space charge limiting current. The current density– voltage dependence in these films was found to obey the following relation,

$$J = \frac{9}{8}\varepsilon\mu\frac{V^2}{d^3}$$

By using an ellipsometer, we found that the thickness of Alq_3 and PVK layers equal to 18 nm and 48 nm respectively. We plotted the variation of the refractive index curves of Alq_3 and PVK thin films on Si as a function of wavelength (visible spectrum) at 75^o angle of incidence. The variation of the refractive index of Alq_3 and PVK thin films with wavelength (visible spectrum) were plotted using Origin 5.0 from Microcal Software, Inc. These curves show that refractive index–wavelength dependence obey Cauchy relation. We calculated the values of three parameters A, B, and C in Cauchy relation for Alq_3 film on Si wafer and PVK film on Si wafer, as tabulated in table (4.3).

Finally, for other developments and improvements of this work we recommend the following:

1. Clean room condition for preventing the dust from incoming into the sample during preparing.
2. Providing technique for controlling and measuring the thickness of thin film layer and cathode layer.
3. providing means for measuring the wavelength of the emitted electroluminescence.
4. More work is needed to reduce the threshold voltage V_T of these devices using multilayers.
5. More efforts must be done to improve the performance of these devices by varying the dopant concentrations and incorporating additional electron transport layers.

APPENDIXES

Appendix (A)

MOTT- Gurney Steady-State Space- Charge-Limited Conduction Model

$$J = \varepsilon\mu E(x)\frac{d}{dx}E(x) \tag{1.A}$$

By integration with respect to x

$$\int_0^x J dx = \varepsilon\mu\int_0^x E(x)\frac{dE(x)}{dx}dx \tag{2.A}$$

then

$$Jx = \frac{\varepsilon\mu}{2}\left(E^2 + \kappa\right) \tag{3.A}$$

$$E(x) = \sqrt{\frac{2J(x+\kappa)}{\varepsilon\mu}} \tag{4.A}$$

Derive the previous equation with respect to x

$$\frac{\partial E(x)}{\partial x} = \left(\frac{J}{2\varepsilon\mu}\right)^{\frac{1}{2}}\left(\frac{1}{\kappa + x}\right)^{\frac{1}{2}} \tag{5.A}$$

$$\left.\frac{\partial E(x)}{\partial x}\right|_{x=0} = \left(\frac{J}{2\varepsilon\mu}\right)^{\frac{1}{2}}\left(\frac{1}{\kappa}\right)^{\frac{1}{2}} \tag{6.A}$$

At the boundary contacts

$$\frac{\partial}{\partial} E\big|_{x=0} = \frac{N\ e}{\varepsilon} \tag{7.A}$$

Equating equation (6.A) and equation (7.A)

$$k = \frac{J\varepsilon}{2N^2e^2\mu} \tag{8.A}$$

where κ is the integration constant.

For a device of thickness d

$$V = \int_0^d E(x)d(x) = \sqrt{\frac{2J}{\varepsilon\mu}}\left[\int_0^d \sqrt{(x+\kappa)}\right] \tag{9.A}$$

$$V = \sqrt{\frac{2J}{\varepsilon\mu}}\left[\int_0^d (x+\kappa)^{\frac{1}{2}} d(x)\right] \tag{10.A}$$

$$V = \sqrt{\frac{2J}{\varepsilon\mu}}\left[(\frac{2}{3})\left\{(d+\kappa)^{\frac{3}{2}} - \kappa^{\frac{3}{2}}\right\}\right] \tag{11.A}$$

$$V = \sqrt{\frac{8J}{9\varepsilon\mu}}\{(d+\kappa)^{\frac{3}{2}} - \kappa^{\frac{3}{2}}\} \tag{12.A}$$

Appendix (B)

Reflection and Transmission by a Single Film

$$r = r_{o1} + t_{01}r_{12}t_{10}\exp(-2i\beta) + t_{01}r_{12}r_{10}r_{12}t_{10}\exp(-4i\beta) + ... \quad (1.B)$$

$$r = r_{o1} + t_{01}r_{12}t_{10}\exp(-2i\beta)\left(1 + r_{10}r_{12}\exp(-2i\beta) + r_{10}r_{12}\exp(-2i\beta)^2 + ...\right) \quad (2.B)$$

where t is the transmission coefficient and r is the reflection coefficient

From Tayler expansion

$$\frac{1}{1-z} = 1 + z + z^2 + ... \quad , \text{ for } |z| < 1$$

let $z = r_{10}r_{12}\exp(i\beta)$ and substituting from previous sequence into equation (2.B)

$$r = r_{01} + \frac{t_{01}r_{12}t_{10}\exp(-2i\beta)}{1 - r_{01}r_{12}\exp(-2i\beta)} \quad (3.B)$$

After some treatments

$$r = \frac{r_{01} + r_{12}(t_{01}t_{10} - r_{01}r_{10})\exp(-2i\beta)}{(1 - r_{10}r_{12}\exp(-2i\beta))} \quad (4.B)$$

Appling the stock's relation ($r_{10} = -r_{01}$, $t_{01}t_{10} = 1 - r_{01}^2$) in equation (4.B) will given

$$r = \frac{r_{10} + r_{12}(-t_{01}^2 + 1 + t_{01}^2)\exp(-2i\beta)}{\left(1 + r_{01}r_{12}\exp(-2i\beta)\right)} \quad (5.B)$$

Finally

$$r = \frac{r_{01} + r_{12}\exp(-2i\beta)}{1 + r_{01}r_{12}\exp(-2i\beta)} \quad (6.B)$$

For P and S polarizations

$$r_p = \frac{r_{01p} + r_{12p}\exp(-2i\beta)}{1 + r_{01p}r_{12p}\exp(-2i\beta)} \tag{7.B}$$

$$r_s = \frac{r_{01s} + r_{12s}\exp(-2i\beta)}{1 + r_{01s}r_{12s}\exp(-2i\beta)} \tag{8.B}$$

Equations(7.B), and equation (8.B) are called Fresnel's equation for reflectance.

Similarly, the total complex transmission coefficient is

$$t = t_{01}t_{12}\exp(-2i\beta) + t_{01} + r_{12}r_{10}t_{12}\exp(-4i\beta) + t_{01}r_{12}r_{10}r_{12}r_{10}t_{12}\exp(-6i\beta) + ... \tag{9.B}$$

After some treating the complex transition coefficient can be derive as:

$$t = \frac{t_{01}t_{12}\exp(-2i\beta)}{1 + r_{01}r_{12}\exp(-2i\beta)} \tag{10.B}$$

For P and S polarizations

$$t_p = \frac{t_{01p}t_{12p}\exp(-2i\beta)}{1 + r_{01}r_{12p}\exp(-2i\beta)} \tag{11.B}$$

$$t_s = \frac{t_{01s}t_{12s}\exp(-2i\beta)}{1 + r_{01}r_{12s}\exp(-2i\beta)} \tag{12.B}$$

Equation (11.B) and equation (12.B) are called Fresnel's equation for transmission.

REFERENCES

REFERENCES

[1] A. Tag, Physical Chemistry of Polymer, Translation from Russian by David Sobolev and Nicholas Bobrov, Mir publishes, Moscow, 2ed edition (1978).

[2] R. J. Young, Introduction to Polymers, Chapman and Hall Poub. Co., new York, 2ed edition (1998).

[3] T. A. Geissman, Principles of Organic Chemistry, McGraw-Hill pub.Co., New York, 2ed edition (1977).

[4] H. Wittcoff, B. Reuben, Industrial Organic Chemicals, McGraw-Hill pub.Co., New York, 2ed edition (2002)

[5] M G Arora, M Singh, Polymer Chemistry, World Scientific Publishing Company, Columbia (2002)

[6] R. Friend, R. Gymer, J. Burroughes, "Electroluminescence in Conjugated Polymers", Macmillan Magazines, 397, 14, 121-128 (1999).

[7] C. Chiang; Y.Park; A. Sharakawa, " Conjugated Polymer", Phys.Rev. Lett. 73, 108–110 (1998).

[8] R. Fessen den & Joan S. Fessenden, Organic Chemistry, University of Montana, 2ed edition (2001).

[9] C. Wayne and R.P. Wayne, Photochemistry, Oxford Press University (1996).

[10] I. G. Csizmadia, Theory and Practice of MO Calculations on Organic Molecules,
Elsevier pub.Co., Amsterdam (1976).

[11] J.R. Lakowicz, Principles of Fluorescence Spectroscopy, Plenum Press, New York (1983).

[12] T. W. Graham Solomons, Craig B. Fryhle, Organic Chemistry, Wily pub.Co., New York 3ed Edition (1984)

[13] P. W. Atkins and R. S. Friedman, Molecular Quantum Mechanics, Oxford University Press, 3ed edition (1999).

[14] M. A. Baldo, M. E. Thompson and S. R. Forrest1," Phosphorescent Materials for Application to Organic Light Emitting Devices". Pure Appl. Chem., 71, 11-18 (1999).

[15] M. Pope and C.E. Swenberg," Electronic Processes in Organic Crystals and Polymers", Phys. Rev. 59, 4449 (1995).

[16] N. Tessler, Organic Semiconductors and Devices, Technion institute, Haifa (1999).

[17] Peumans, Bulovic, and Forrest.," Exciton Diffusion", Appl. Phys. Lett. 76, 38- 48 (2000).

[18] M. Fox, Optical Properties of Solids, Oxford University Press (2001).

[19] F.W.Billmryer, Textbook of Polymer Science, 2ed edition, Wiley, New York (1984).

[20] W. Rasmussen, Novel Carbazole Based Methacrylates, Acrylates, and Dimethacrylates to Produce High Refractive Index Polymers, Ph.D., Virginia Polytechnic Institute and State University,Virginia (2002).

[21] Tadatstugu Minamin, "New n-Type Transparent Conducting Oxides", MRS Bulletin,38-39 (2000).

[22] D. Ammermann, A. Blhler, W. kowlsky, Device Structures and Material Organic Light Emitting Diodes, Institute für- Hochfrequenztechnik, Tu., 9-12 (1996).

[23] Ph. R. Draviam, Masters Thesis, Characterization of Organic Light Emitting Diodes Using an Aluminum/Rare-Earth Sulfide Bilayer Cathode, Master of Science Thesis, University OF Cincinnati (2005).

[24] Jinkoo Chung, Beomark Chio, and Hong H. Lee, "Polyaniline and PVK Blends as for Blue Light-Emitting Diodes" , Appl. Phys. Lett., 24, 14 3646 (1999).

[25] S.M.Sze, Physics of Semiconductor Devices, 2ed edition, Wiley&sons, (1999).

[26] R. Muller and T. I.Kamins, Device electronics for integrated Circuits, 2ed edition, Wiley & sons (1997).

[27] W. Brutting, S. Berleb, "Space Charge Conduction With A field and Temperature Dependent Mobility in Alq Light- Emitting Devices",Synth. Met., 122, 99- 109(2001).

[28] Y. Pereezant, Electrical Properties of Contact Region of Polymeric Semiconductor Devices, Master thesis, Technion–Israel Institute of Technology, Haifa (2004).

[29] R .Coelho, Physics of Dielectrics for The Engineer, Pub. Co., Amsterdam

(1997).

[30] P. W. M. Blom, M. J. M. dejong, J. J. M. Vleggar, Electron and Hole Transport in Poly (9-phenylene vinylene) Devices, Appl. Phys. Lett., 68, 23 ,3304-3308 (1996).

[31] Sh. Wagle and Vinay Shirodkal, SCLC in Thin Film Al/Sb_2PbSe_7/Al, Braz. J. Phys., 2 São Paulo (2000).

[32] Ch. Scott, Overview of Spin Coating, Department of Material Science and Engineering, Massachusetts Institute of technology, Tokyo (2000).

[33] K. Garre, Investigation of the Use of Rare-Earth Sulfide Thin Film as Efficient Cathodes in Organic Light Emitting Diodes, Master of Science thesis, University OF Cincinnati, Cincinnati (2004).

[34] S. Akcay, "Building Light Emitting Devices Based on Polymeric substrates", College of William and Marry, REU Summer Program, National Science Foundation,Ohio (2000).

[35] J. Kraus and Daniel Fleisch, Electromagnetic, Mc Graw-Hill, London (1999).

[36] P. Lorrin and Dale Corson, Electromagnetic Fields and Waves, New York (1999).

[37] F.G.Smith and J.H.Thomson, Optics, The Manchester Physics Series, Chichester Wiley&, 2nd edition (1988).

[38] H. G.Tompkins, A User's Guide to Ellipsometry, Academic Press, INC., 1st edition, Boston (1993).

[39] R.M.A. Azzam, and N.M. Bashara, Ellipsometry and Polarized Light, North Holland Press, New York,1st edition (1993).

[40] T. M. ElAgez, Characterization of A rotating Polarizer and Analyzer Ellipsometer, for The Study of The Plasma Polymerized Film, PhD. Thesis, University of Missouri, Kansas City (1999).

[41] S. Samuel, "An Absorbing Surface Film on An Absorbing Substrate With or Without An Intermediate Surface Layer", Surface Science 56, 97-108 (1976)

[42] F.A.Jenkins and H.E White, Fundamental of Optics, McGraw-Hill, Inc., New York, 4th edition (1981).

[43] S. Ouro Djobo, J.C Bernede, S Marsillac," Poly (N-vinylcarbazole) (PVK)

Deposited for Light Emitting Diodes Thin Films Structures", Synthetic Metals, 122, 31-133 (2001).

[44] B. J. Norris, Low Cost Deposition Methods for Transparent Thin-Film Transistors, Ph.D. Thesis, Oregon State university, Corvallis (2003).

[45] M. Stössel, A. G. Seimens, G. Wittmann, K. Heuser, J. Blässing, and M. Proc. Inbasekaran, SPIE, 4105 (2001).

[46] J. Kima, Sokwon Noha, Kwanju Kimb, Sung-Taek Lima, Dong-Myung Shina, Synthetic Metals 117, 227-228 (2001).

[47] C.H. Leea, G.W. Kanga, J.W. Jeona, "Blue Electroluminescence and Dynamics of Charge Carrier Recombination in A vacuum-Deposited Poly(p-phenylene) Thin Film", Thin Solid Films 363, 306-309 (2000).

[48] F. Michelotti, F. Borghese, M. Bertolotti, "Alq_3/PVK Hetrojunction Electroluminescent Devices", Synthetic Metals, 111, 112, 105–108 (2000).